UNIVERSIDADE D
COIMBRA

André Miguel Goulart Ferreira Batalhão Ramos

DESIGN OF A COOLING SYSTEM FOR AN ALL-TERRAIN ELECTRIC VEHICLE FOR FIREFIGHTING

Dissertação no âmbito do Mestrado em Engenharia Mecânica, na área de Energia e Ambiente, orientada pelo Professor Doutor Carlos Xavier Pais Viegas, coorientada pelo Professor Doutor Adélio Manuel Rodrigues Gaspar e apresentada ao Departamento de Engenharia Mecânica da Faculdade de Ciências e Tecnologia da Universidade de Coimbra.

Fevereiro de 2023

1 2 9 0

FACULDADE DE CIÊNCIAS E TECNOLOGIA
UNIVERSIDADE D COIMBRA

Design of a cooling system for an all-terrain electric vehicle for firefighting

A dissertation submitted in partial fulfilment of the requirements for the degree of Master in Mechanical Engineering in the speciality of Energy and Environment

Projeto de um sistema de arrefecimento para um veículo elétrico todo-o-terreno para combate a incêndios

Author

André Miguel Goulart Ferreira Batalhão Ramos

Advisors

Prof. Dr. Carlos Xavier Pais Viegas

Prof. Dr. Adélio Manuel Rodrigues Gaspar

Committee

Chair	**Professor Doutor António Manuel Gameiro Lopes** **Professor Associado da Universidade de Coimbra**
Members	**Professor Doutor Miguel Rosa Oliveira Panão** **Professor Auxiliar da Universidade de Coimbra** **Professor Doutor Almerindo Domingues Ferreira** **Professor Auxiliar da Universidade de Coimbra**
Advisor	**Professor Doutor Carlos Xavier Pais Viegas** **Professor Auxiliar Convidado da Universidade de Coimbra**

Institutional Collaboration

Association for the Development of Industrial Aerodynamics

Bold Robotics Lda.

Coimbra, February, 2023

ACKNOWLEDGEMENTS

The work presented and the journey to get here was only possible thanks to the collaboration and support of some people, to whom I must express my gratitude.

To my advisor, Professor Doctor Carlos Xavier Pais Viegas, for his constant willingness, help and support during this period. For his guidance and for making sure I felt like I was part of his team.

To my co-advisor, Professor Doctor Adélio Manuel Rodrigues Gaspar, for his constant availability throughout this period. Helping whenever I felt stuck in the course of the work.

To the Field Tech Laboratory team for welcoming me as part of the team. Especially, Miguel Gaspar for the immense advice throughout this time.

To the best friends in the world, for showing me the true value of friendship and for never giving up on me.

To my new family from Porto, for treating me like a member of the family from day one. A special mention for my borrowed grandmother, Laidinha, who always gave me a lot of strength for this day to come.

To my siblings, Ana, Leonor and Tiago, for letting me be their big brother and for making my world happier.

To my grandparents, Lubélia, Eugénia, António and Abel and uncles Sofia, Cláudia, Rui and Sérgio, for all the love and support they have always given me.

To my parents, Margarida and Pedro, for never giving up on me, even when it seemed the easiest thing to do. For all the love and support they have given me and for making me feel like the luckiest son in the world.

Finally, to Ana, the love of my life, the person who «saved» my life. For all the help and motivation, for being there every time I needed, for all the anger and laughter. And above all, for loving me and making me wish and long for the future.

Abstract

In the current context, the increase in wildfires is a growing concern worldwide, as they can cause significant damage to property, communities, and ecosystems. In addition, firefighters continue to be exposed to the inherent dangers of wildfires.

All this means that firefighting and fire prevention robots are a growing reality. Not only do robots take some risk away from firefighters, as they are also more efficient.

Since a robot is made up of several electrical components, it is very important that these components perform well, are reliable, and last a long time. These characteristics depend mainly on temperature, which makes it extremely important to ensure that the electrical components operate within certain temperature ranges, especially when the robot is in a fire situation, where temperatures are high.

This dissertation aims to contribute to the development of a 100% electric autonomous all-terrain vehicle, designing a cooling system that allows the vehicle to perform forest management functions, but above all that can operate in high temperature conditions.

This work starts with a state-of-the-art investigation of the different cooling strategies for the electric components, batteries and electric motors, and possible cooling systems.

Based on the research, a cooling system was devised. Based on this system, calculations were performed, which led to the choice of the necessary components for the proposed system. In addition, a proposal was made for the control system capable of meeting the needs of the cooling system.

Keywords: Robot, Autonomous, Firefighting, Cooling System, Electric Motors, Batteries.

Resumo

No contexto atual, o aumento dos incêndios é uma preocupação crescente a nível mundial, uma vez que podem causar danos significativos a propriedades, comunidades e ecossistemas. Aliado a isto, continua-se a assistir a uma exposição enorme, por parte dos bombeiros, aos perigos inerentes provocados pelos incêndios.

Tudo isto, leva a que os robôs de combate e prevenção a incêndios, sejam uma realidade cada vez maior. Não só os robôs retiram algum risco aos bombeiros, como também são mais eficientes.

Sendo um robô, constituído por diversos componentes elétricos, é muito importante que esses componentes possuam um bom desempenho, fiabilidade e durem bastante tempo. Estas características dependem principalmente da temperatura, o que torna de extrema importância, garantir que os componentes elétricos operem entre determinados intervalos de temperatura, principalmente quando o robot está em situação de incendio, onde as temperaturas são elevadas.

Esta dissertação tem como objetivo, contribuir para o desenvolvimento de um veículo 100% elétrico autónomo todo-o-terreno, concebendo um sistema de arrefecimento que permita o veículo desempenhar funções de gestão florestal, mas acima de tudo que consiga operar em condições de temperaturas elevadas.

Este trabalho inicia com uma investigação do estado-de-arte sobre as diferentes estratégias de arrefecimento dos componentes elétricos, baterias e motores elétricos, e possíveis sistemas de arrefecimento.

Foi idealizado um sistema de arrefecimento, com base na investigação feita. Com base nesse sistema, foram realizados cálculos, que levaram à escolha dos componentes necessários para o sistema proposto. Além disso, foi feita uma proposta para o sistema de controlo capaz de satisfazer as necessidades do sistema de arrefecimento.

Palavras-chave: Robô, Autónomo, Combate a incêndios, Sistema de arrefecimento, Motores elétricos, Baterias.

Contents

LIST OF FIGURES

LIST OF TABLES

LIST OF SIMBOLS

A– Area

β– Volumetric expansion coefficient

C– Constant

C_p– Specific heat

ΔT– Temperature difference

D– Diameter

η– Efficiency

f– Friction factor

g– Gravity

h– Heat transfer coefficient

H– Manometric height

I– Current

k_f– Fluid thermal conductivity

L– Length

m– Constant

ν– Kinematic viscosity

Nu– Nusselt number

P– Perimeter

P_{in}– Power input

Pr– Prandtl number

q– Power

$\dot{Q}$– Volumetric flow rate

R– Resistance

Ra– Rayleigh number

Re– Reynolds number

ρ– Density

T– Temperature

u– Velocity

W – Width

1. Introduction

Every year, wildfires across Portugal and the globe devastate the land they burn, destroying entire ecosystems, infrastructures and killing people. In Portugal, just in the short period of January 1st to October 15th of 2022, a total of 10449 fires were accounted, resulting in 11007 hectares of burned area. The following figure(Figure 1.1) shows the distribution of the burned territory across the country during this time interval[1].

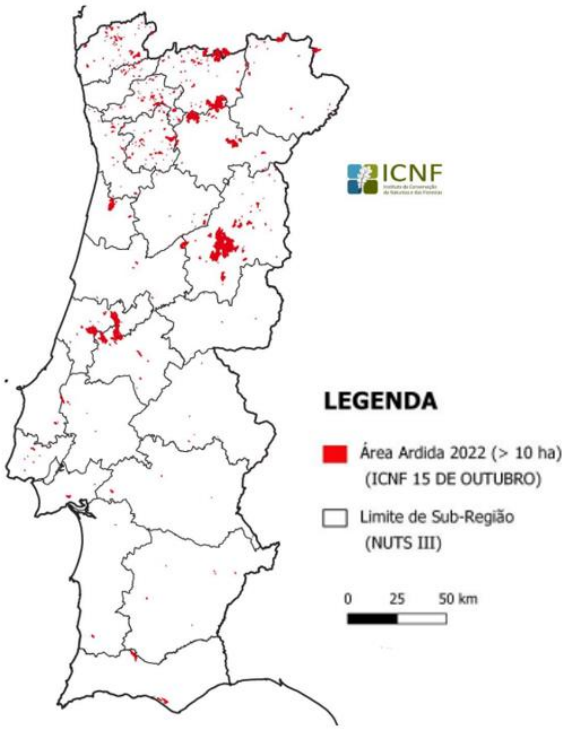

Figure 1.1 - Burnt Areas Distribution in Portugal Continental in 2022[1]

Globally speaking, forests represent 4.06 billion hectares, which corresponds to 31% of the world land area, making this an even more urgent matter[2]. And according to[3], between 1998 and 2017, nearly 3.5% of global disasters were linked to wildfires. Having in account this alarming information and the fact that things don't get better as the years pass by, a solution that can both prevent and "fight" wildfires and at the same time assure the safety of firefighters is needed more than ever.

The project E-Forest was created to try and solve this problem. It consists of an autonomous all-terrain electric vehicle to be used in forest management and firefighting activities. The current thesis presents the design and implementation of a cooling system for

this vehicle, taking into account the components good performance and aiming at the same time to minimize the energy consumption. The project E-Forest results from a coalition between the University of Coimbra, Jacinto Marques de Oliveira and Bold Robotics Lda. In this chapter, we discuss the motivation behind this thesis, mainly focused on a firefighting situation, which is the main challenge of this project, followed by a brief introduction to the vehicle itself and at last a brief outline of the chapters which will be better explained later on.

1.1. Motivation

An approach to a fire event can be done in two perspectives, fire prevention and firefighting, and the E-Forest autonomous vehicle was built based on both requirements.

Being a 100% electric vehicle, which means its batteries, electronics and motors are electric, it is very important to guarantee good operational temperatures, to assure better and long-lasting performances from its components, since they are very sensitive to temperature. The forest management scenario isn´t that problematic to the implementation of a cooling system. On the other hand, it´s much more challenging to implement a cooling system in a firefighting scenario, where the environment temperatures will be very high. This is the first and main purpose for the work presented in this thesis.

There is a large amount of literature regarding the appliance of cooling strategies to the electric components individually, especially batteries and electric motors, these being the most important components, but there is a lack of information about an integrated system that contemplates both of them together. This is the second aim for the work in this thesis.

1.2. Objectives

The primary goal of this dissertation is to implement a cooling system for an autonomous vehicle for forestall management and firefighting. To complete this goal, a few steps were proposed. To start, a state-of-art, for a better understanding of the subject, should be done.

After that, the project of the cooling system and selection of components must be done. After that, the development of a software of the control system, has to be done for the good functioning of the system. Finally, the cooling system has to be tested in lab environment and then tested on the vehicle prototype.

1.3. Outline

This thesis is organized as follows. In the 2nd chapter, a state-of-the-art about cooling systems applied to electric components (batteries and motors) is presented, mentioning also some existing firefighting robots. The 3rd chapter details the conception of the cooling system components, as well as the calculation methodologies and approaches. Also, a proposal for the control system is made. The 4th chapter includes the results and selection of the cooling system components. Finally, in the 5th chapter we present and discuss our conclusions, along with some suggestions for future work.

2. State-of-Art

This chapter presents the recent advances in robots used for firefighting applications. Furthermore, the current state-of-art in cooling systems, mainly focused on cooling strategies applied to batteries and motors is also presented. It starts by explaining the various already existing strategies, their advantages and limitations, allowing a comparison between them. These are followed by demonstrating some experimental research regarding each of the strategies mentioned.

2.1. Firefighting Ground Robots

Firefighting robots result from the urgent need of reducing firefighters' exposure to danger. Being a mechanical structure, they can be very resistant to high temperatures and concentration of gases and dust scenarios, and have the advantage of carrying large amounts of water or equipment. Thereby, they can also assure a faster, safer and more efficient way of spraying water or delaying external agents in forest regions. The following pictures shows some of these robots.

Figure 2.1 - Fire Ox[4]

Fire Ox[4] was created by Lockheed Martin. It is a 6-wheel semiautonomous military vehicle adapted for firefighting purposes. It possesses a 250-gallon (946 liters) tank and a 1000 Watts electrical generator. This robot can be handled using a remote control with RGB and infrared cameras. The autonomous technology of the robot can help with hazmat (hazardous materials) situations, injury evacuation and trenching, among others.

Figure 2.2 - Multiscope Rescue with hydra (left)[5] and hose cartridge (right)[6]

Multiscope Rescue with hydra[5] and hose cartridge[6] were both developed by Milrem Robotics. The hydra vehicle is used in extinguishing fires and the hose cartridge is used to assist in the transportation of hoses in dangerous and difficult access scenarios, like warehouses and tunnels. The first one can shoot 3000 liters per minute of foam and/or water with a maximum range of 62 meters. None of these robots are able to carry water, and they must be connected to a water source through a firefighting hose.

Figure 2.3 - Colossus[7]

Colossus[7] was announced by Shark Robotics in 2017. It was built to be as modular as possible. Regardless of the situation, the robot takes less than 30 seconds to be adapted to the new necessary form, without the need of additional tools. It is always operated remotely by a trained firefighter. Similarly, to the previous solutions from Milrem Robotics, it does not carry water.

Figure 2.4 - RTE robot[8]

RTE robot[8] was developed by Rosenbauer. It was specially created for the use of fire departments and emergency services. It is a multi-functional, wireless remote control,

electric vehicle from the crawler type, that can carry up to 650 kg of cargo. It can function to transport things or to firefighting. In firefighting scenario, it can eject 3800L/m at throw ranges of 80m.

Figure 2.5 - Magirus Wolf RI[9]

Magirus Wolf RI[9] was invented by Magirus. It was designed to for a wide range of applications, such as firefighting operations, firefighting support, hazardous substance detection and logistics tasks. It can expel up to 2000L/m with throwing distances of 65m for water and 45m for foam.

Figure 2.6 - Dronster[10]

Dronster[10] was created by Vallfirest. It is a remote-control emergency robot for forest management and to perform indirect wildland fire attacks, structural fires and rescue operations. It is adapted to pass through irregular and sloped grounds.

Figure 2.7 - MVF-5[11]

MVF-5[11] was conceived by DOK-ING. It is a multi-function robot, that can operate under hard, demanding and threatening conditions. Its main functions are fire extinguishing and clearing roadblocks and debris.

Robot	Manufacturer	Mass (Kg)	Lenght and width (m x m)	Water carrying capacity (L)	Motor power (kW)
Fire Ox	Lockheed Martin	No info	No info	946	No info
M.S. Hydra	Milrem Robotics	1630	2.4 x 2	None	No info
Colossus	Shark Robotics	525	1.6 x 0.78	None	2 x 4
RTE robot	Rosenbauer	350	1.2 x 0.8 or 1.07	None	No info
Magirus Wolf RI	Magirus	Up to 900	1.5 x 1.2	None	2 x 7.5
Dronster	Vallfirest	850	1.71 x 0.887	None	24.5
MVF-5	DOK-ING	16000	5.75 x 2.28	2500	186 or 205

Table 1 - Comparative table between the referred robots

2.2. Batteries Thermal Management Systems

2.2.1. Batteries

The lithium-ion batteries are the most commonly used because of their higher energy density, higher specific power, lighter weight, lower self-discharge rates, higher recyclability and longer cycle life compared to others like lead-acid, nickel–cadmium (Ni-Cd) and nickel-metal hydride (Ni-MH) batteries[12]. According to[13] the batteries are the most important part of electric vehicles (EVs). They are very sensitive to temperature, as it can easily affect their performance and stability. Having this in mind, an efficient BTMS (Battery thermal management system) is necessary to maintain the proper temperature within certain limits, in order to mitigate the temperature variation across the battery multiple modules and avoid accidents[14]. Having these in account a lot of experiments were made to understand the ideal temperature characteristics of the batteries. Recently, Jiang et al.[15] claimed that the ideal operating temperature range should be maintained between 20 °C and 45 °C and for

some time now, Pesaran et al.[16] came to the conclusion that the maximum temperature difference from module to module should be lower than 5 °C.

2.2.2. Classification Of Battery Cooling Systems

BTMS, as mentioned before, is a cooling system used to keep the operating temperature of the batteries within certain limits, so that their performance and stability are not affected and also to prevent thermal runaway.

According to Pesaran[17] BTMS needs to have four different requirements:

- Cooling, to remove the heat from the battery;
- Heating, in low temperature scenarios;
- Insulation, to prevent sudden temperature change of the battery;
- Ventilation, to exhaust the potentially hazardous gases from the battery.

The BTMS can be classified accordingly to power-consumption, working fluid and arrangement. The next figure (Figure 2.8) is a demonstrative scheme of that.

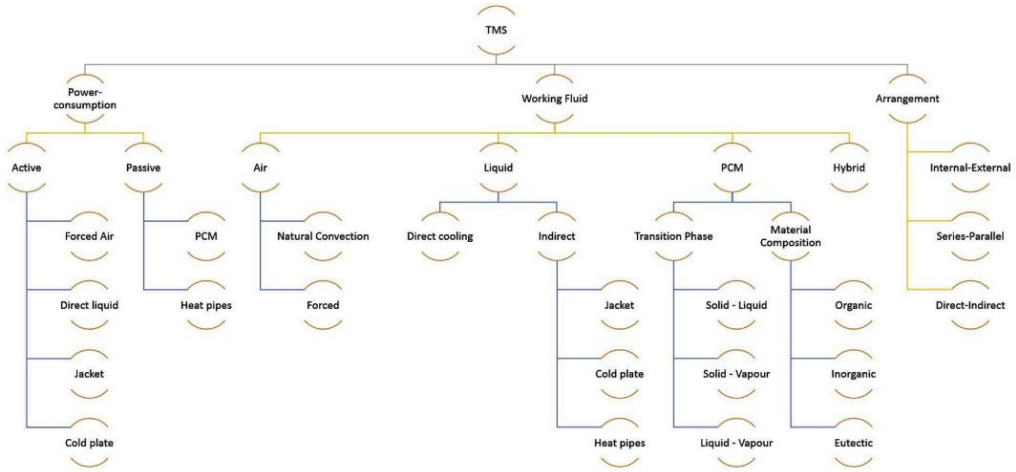

Figure 2.8 - Classification of Batteries thermal management strategies[18]

From a working fluid perspective, we have three major types of BTMS:

- Air-cooling;
- Liquid-cooling;
- PCM.

There are other cooling strategies, like Thermoelectric cooling, but seemingly not very appealing to BTMS researchers.

2.2.2.1. Air-Cooling Strategies

Air-cooled BTMS uses air as a working fluid. In these systems, the air gets in contact with the batteries, by means of fans and manifolds (Forced convection).

Advantages of Air-cooling systems:

- Simple design;
- Low operating cost;
- Low maintenance cost.

Disadvantages of Air-cooling systems:

- Low thermal conductivity;
- Low heat transfer capability;
- Too much noise, caused by the fans.

Air cooling can use two different approaches, natural and forced convection (Figure 2.9). Natural convection is easier to implement. However, it is not enough for it to be equated for BTMS, because of its low heat transfer coefficient. It can't fulfill the cooling requirements under hot temperatures, large battery packs or under high charge-discharge cycles[19]. To surpass these drawbacks, forced convection, through the use of exhaust fans or blowers, is the most obvious choice for air-cooling systems.

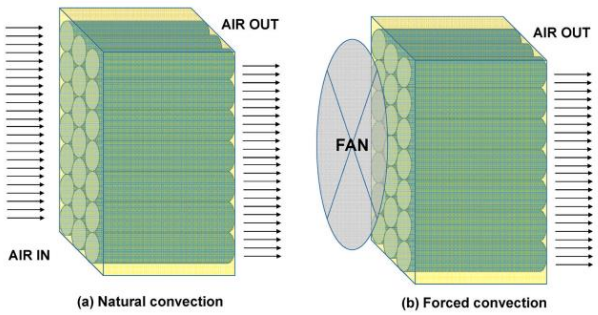

Figure 2.9 - Air cooling strategies for batteries: (a) Natural convection, (b) Forced convection[20]

Several research and experiments were done to establish the efficiency of this cooling strategy. For example, based on varying the airflow channels and parameters, Yuanzhi Liu et al.[21] suggested a J-type air-cooling BTMS where the temperature uniformity can be increased by alternating the mode of operation between U-type and Z-type structures supported by 2 control valves. The optimized results showed that, for the J-type structure, the temperature rise decreased by 31.18%.

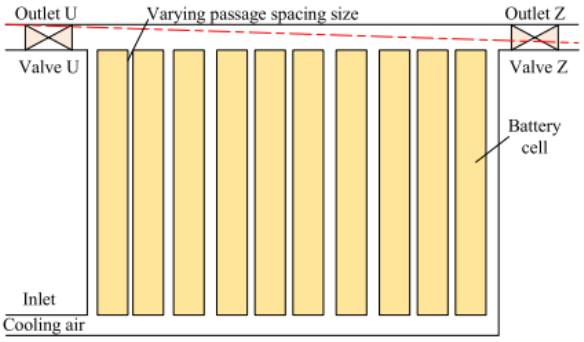

Figure 2.10 - Conceptual design of a J-type air based BTMS[21]

Na[22] compared reverse stratified airflow and unidirectional airflow to study the temperature distribution. They reached the conclusion that reverse airflow can substantially increase temperature uniformity in the battery module, reduce overall maximum temperature difference and reduce maximum average temperature difference. Saw[23] by analyzing an air-cooling system on a battery module, showed that when the airflow increases, the heat transfer coefficient and the pressure drop increase too. Hong[24] found out that the temperature rises and the temperature changes of the battery module were independent from the air inlet temperature, but were proportional to the heating rate of the battery module. Based on fin structure, Shahabeddin K. Mohammadian et al.[25] designed a pin fin heat sink-based air cooling for a prismatic Li-ion battery pack and concluded that it decreased not only the temperature but also the temperature variation across the battery pack. Also, focusing on the cell configuration, Xiaoling Yu et al.[26] studied a staggered battery pack with natural and forced air cooling and realized that to increase the lifecycle of the battery, forced air cooling with longitudinal flow should be adopted. In another research, Chen[27], presented an optimal solution under a constant heat rate, based on the spacing between battery cells. The results show that it improved parallel air-cooling performance. It also slightly reduced the maximum temperature and the maximum temperature difference by 42% of the battery pack. The battery pack is composed by 2x12 battery cells and the spacings of the optimized solution are [1.7, 2, 2.3, 2.3, 2.1, 2.1, 2.1, 2.1, 2, 2, 2, 2, 1.3] mm. Also, the spacing around the battery cell with the highest temperature should be increased, while the spacing around the battery cell with the lowest temperature should be decreased.

2.2.2.2. Liquid-Cooling Strategies

Liquid-cooled BTMS uses liquid as working fluid. They can be classified as:

- Direct liquid cooling;
- Indirect liquid cooling.

Advantages of liquid-cooling system:

- higher heat capacity and thermal conductivity, when compared to air-cooling systems;
- Can be 3500 times more effective than air and save up to 40% parasitic energy;
- Reduced noise level;
- Compactness without reducing the efficiency.

Disadvantages of liquid cooling system:

- Complexity of the system;
- High costs;
- Potential for leakage.

2.2.2.2.1. Direct Liquid-Cooling

Is done by the immersion of the batteries in a liquid (working fluid). In comparison with indirect cooling, direct cooling has the capacity to cool the entire surface of the battery, which helps to keep an uniform temperature in the battery[28]. However, it raises several issues, like electrical short circuit and electrochemical corrosion, which probably explains why this method isn´t widely applied to BTMS.

2.2.2.2.2. Indirect Liquid-Cooling

In this option, the fluid doesn't get in direct contact with the batteries. Instead, it's done by transferring the heat from the batteries to the fluid (convection), through a solid material (conduction), usually metal.

They can be divided into two major strategies:

- Heat pipes;
- Cold plate-based cooling.

2.2.2.2.2.1. Heat Pipes

A thermal management system with heat pipes is a passive system moved by the capillary action of a wick material coating the internal surface of a vacuum-sealed shell. It removes heat during the working fluid phase change, from liquid to vapor. In more detail, the liquid inside the wick absorbs the heat excess from the battery cells which are arranged in the hot extremities of the heat pipe, and evaporates. Then, the increased vapor pressure and small molecular density originate a pressure gradient in the pipe that guides the hot vapors to the condensing section, where heat is rejected to the heat exchanger. The capillary forces developed in the wick guide the condensed liquid to the evaporator again[29]. Some of the fluids normally used are water, acetone, methanol and ammonia, depending on the characteristics of the shell[30].

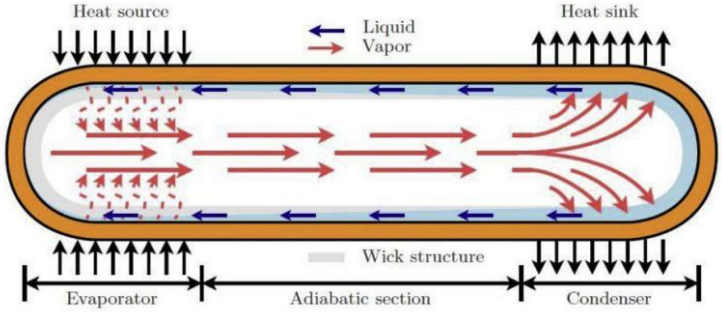

Figure 2.11 - Schematic of a traditional heat pipe with tubular structure and closed ends[29]

Advantages of heat pipes:

- Don't need pumped power, which means less components, so less cost;
- Compactness;
- Flexible geometry;
- Long life;
- Low maintenance.

Disadvantages of heat pipes:

- Low capacity;
- Low efficiency;
- Small area of contact.

Focusing on this strategy, Mahefkey et al.[31] and Zhang et al.[32] studied different batteries with heat pipes incorporated and both of them reached the conclusion that the usage of heat pipes can mitigate any thermal excursions in the battery pack.

Swanepoel[33]investigated the possibility of using a pulsating heat pipe and ammonia as the working fluid. After some experiments, they realized that by using a PHP with a diameter inferior to 2.5mm, a good temperature uniformity can be achieved. Also, they also confirmed that heat pipes can keep the operating temperature of the battery in a safe range.

2.2.2.2.2.2. Cold-Plate Cooling

Cold plate cooling systems are used preferably when there are space limitations. Essentially, they generally consist of a metal block, usually aluminum or copper, with channels built inside for a liquid coolant to circulate and carry the absorbed heat from the battery, by direct contact between the cold plate and the battery. Evaluation of cold plate performance is made in terms of the heat transfer rate and the thermal distribution across the module, its power consumption depending upon the convective heat transfer coefficient between the plate and the liquid coolant, or the coolant flow rate and ambient temperature[18]. Different channels designs and geometries can be required, depending on the requirements of the system. Cold plate cooling can be divided in two scenarios:

- **Fin cooling**

This method is very effective in maintaining the equal temperature at the cell level, by readjusting the generated heat flux in the fuel cell equally through fins and highly conductive thermal liquid. Limitation-as the liquid is flowing in a single coolant and is cooled with the help of front fins only, the performance of this method decreases slowly, as the temperature difference between the liquid and the fin used is slowly decreased[34].

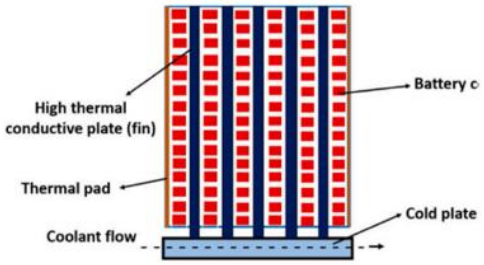

Figure 2.12 - Fin cooling strategy for batteries[20]

- **Mini channel cold-plate cooling**

The temperature uniformity in the cell is very uniform compared to the fin cooling method. Limitation- needs a long and narrow channel that results in the high-pressure drop;

Solution- using an electric coolant pump with the inbuilt characteristics of having high flow rates and static pressure[34].

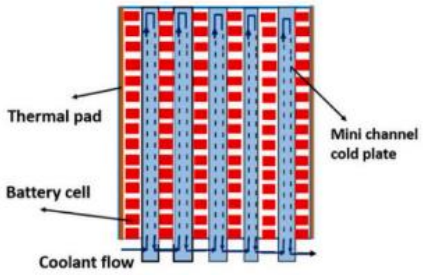

Figure 2.13 - Mini channel cold-plate cooling for batteries[20]

Several studies were made based on this cooling strategy. Deng[35] reached the conclusion that cooling plates were suited to square and pouch batteries and can work as jackets for cylindrical batteries. Wang[36] conceived a new solution based on silica gel plates. The combination of this plates with the water results in a feasible and effective composite liquid cooling system. The results show that maximum temperature was reduced to 48.7ºC and the maximum temperature difference was maintained under 5ºC, when the water flow rate was increased to 4ml/s. Yu[37], Choi[38] and Chen[39] confirmed that channel configuration is also a parameter that affects the performance of a cold plate. They can be grouped as serpentine, parallel and multi-channel configurations. Fisher and Torrance[40],[41]studied 3 different channel geometries (rectangular, diamond-shape and elliptical channels) and found out that the rectangular shaped is the most efficient of the three. They also discovered that although more elliptical channels can be accommodated in the same packaging space, the heat transferred is still 5% lower than in rectangular channels. Jarret and Kim[42] studied cold plates with serpentine channels. According to CFD analysis, increasing the width of the channels will reduce the maximum average temperature and the pressure drop of the coolant. On the other hand, small inlets that gradually widen towards the outlet are best at maintaining the temperature uniformity across the battery pack.

2.2.2.3. PCM Cooling Strategies

PCM, also known as phase change material, is a material that absorbs or releases heat by changing its physical state, at a certain temperature. Can absorb or emit huge amounts of heat, without the consumption of energy. Generally, it consists of a solid material block manufactured in a way that the batteries can be inserted inside the block, as shown in the following figure (Figure 2.14).

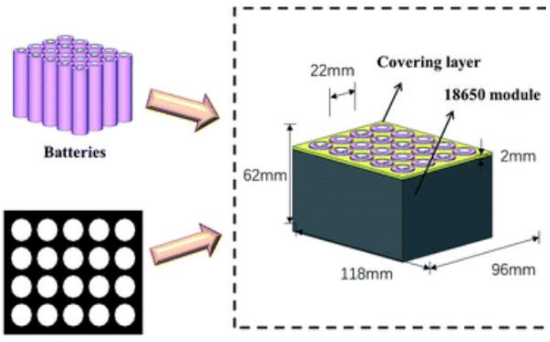

Figure 2.14 - PCM battery cooling strategy illustration[43]

The heat is absorbed from direct contact (conduction) from the batteries. In a first instance, the PCM absorbs sensible heat and then absorbs huge amounts of latent heat until the conclusion of the phase change process at a constant temperature. It stops when it reaches the melting point as the temperature gradually increases. The heat is then released to plates placed in the extremities of the PCM[34].

Advantages of PCM cooling system:

- Low complexity, compared to liquid cooling systems;
- Low power consumption, compared to liquid cooling systems;
- Low maintenance.

Disadvantages of PCM cooling system:

- Difficult to operate alone under hot weather, which makes it necessary to use additional cooling systems, adding more weight and cost;
- Low thermal conductivity;
- Possible leakage;
- Weak mechanical properties;
- Low surface heat transfer between the PCM and the exterior environment.

To prove the value of this strategy, Khateeb et al.[44] studied a battery pack filled with a mixture of PCM and aluminum foam. They concluded that with PCM, they could reduce the temperature rise by half. Mills et al.[45] simulated a laptop battery pack and realized that by using expanded graphite saturated with PCM, they could achieve uniform distribution of the temperature. Kizilel et al.[46] tested a battery pack filled with PCM and found out that temperature uniformity distribution could be achieved either in normal or extreme test conditions.

2.2.2.4. Thermoelectric Cooling Strategies

Thermoelectric coolers are, basically, zero maintenance heat pumps with no moving parts. They use semi-conductor elements, composed by p and n-type thermo-elements, sandwiched in substrates, which are thermally conductive but electrically insulating, to transfer heat through a junction of two different materials through the Peltier effect[47].

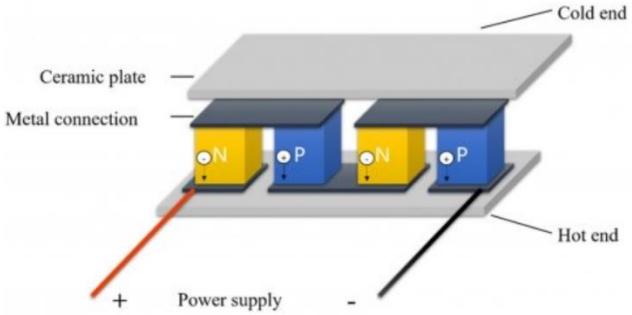

Figure 2.15 - Illustration of a thermoelectric cooling module[48]

Advantages:

- Compactness;
- Lightweight;
- Zero noise and vibrations;
- High precision of the temperature control, margin errors of ± 0.1 °C;
- Low manufacturing costs;
- Big window operation range;
- Possibility of cooling below ambient temperature;
- It is location independent, and can operate in any spatial orientation, at high G-levels or in zero gravity.

Disadvantages:

- Maximum COP (coefficient of performance) is limited to around 10%, which is extremely low.

It still isn't a very explored solution for the BTMS, but studies were already conducted. For example, Liu et al.[49]combined thermoelectric coolers with liquid cooling and it showed that even under high ambient temperatures, the battery was kept in optimum range.

2.2.3. Typical Cooling Systems For BTMS

Here, is a visual presentation of how each cooling system cycle is made, also showing the typical components of each system. The green lines represent the fluid circulation and the blue lines the refrigerant circulation.

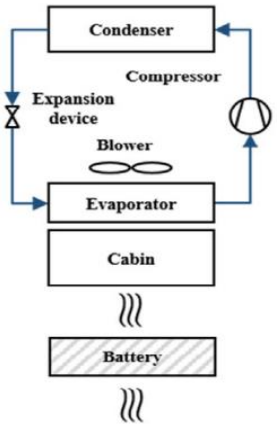

Figure 2.16 - Air cooling system[34]

In Figure 2.16, a typical air-cooling system is presented. A refrigeration cycle is used (compressor, condenser, expansion valve and evaporator). The cooled air in the evaporator is blown, through a blower or a turbine, to the battery.

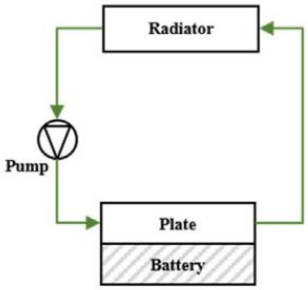

Figure 2.17 - Radiator liquid cooling system[34]

In Figure 2.17, a typical radiator liquid cooling system can be seen. The pump circulates the fluid through a cold plate that cools the battery, by absorbing the heat, and the fluid later on reaches the radiator (heat exchanger), where the heat is released, by exchanging the heat with the outside air.

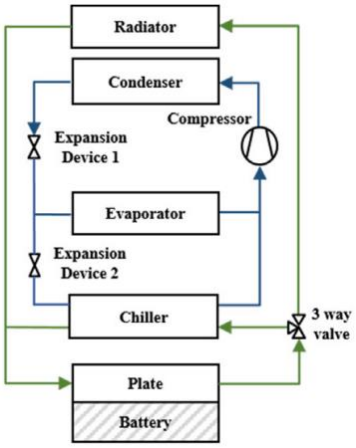

Figure 2.18 - Second loop liquid cooling system[34]

In Figure 2.18, in comparison to Figure 2.17, a refrigeration cycle is added, which is called a secondary loop liquid cooling system. This system is an improvement of the system in Figure 2.17, as it can also be used under high environment temperatures. Of course, it has his drawbacks, namely an additional cycle which brings more components, more weight and turns it into a more complex system to implement. When the environment temperature is lower than the coolant temperature, the system works exactly like in Figure 2.17. But when the environment temperature is higher than the coolant, the coolant flows to the chiller to exchange the heat with the refrigerant in the refrigeration cycle.

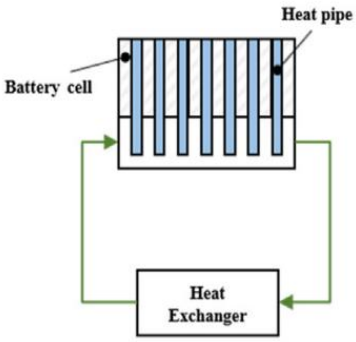

Figure 2.19 - Heat Pipe cooling system[34]

In Figure 2.19, a heat pipe cooling system is visible. This is a relatively simple cycle, as only a heat exchanger is needed in addition to the heat pipes.

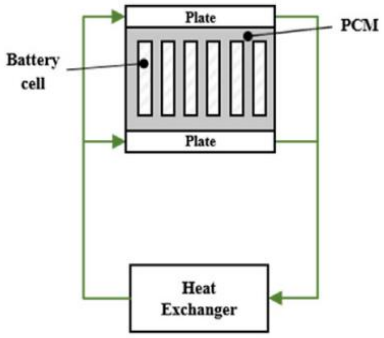

Figure 2.20 - PCM cooling system[34]

In Figure 2.20, the PCM (Phase Change Material) cooling system is found. As is shown in the picture, the PCM that covers the battery is sandwiched by two cold plates that allow the heat transfer to the fluid, and it then goes to the heat exchanger to free that heat.

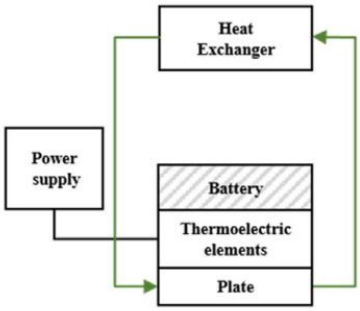

Figure 2.21 - Thermoelectric cooling system[34]

In Figure 2.21, a thermoelectric element cooling system can be visualized. That element uses the Peltier effect, converting electricity into thermal energy. Later, it transmits the heat to a cold-plate that drives the fluid to the heat exchanger.

2.3. Motor Thermal Management Systems

2.3.1. Electric Motors

Electric motors can be classified, according to the type of power source, as DC (Direct Current) motor and AC (Alternate Current) motor. An electric motor converts electrical energy into mechanical energy through the procedure of magnetic induction and it's composed of two main parts: the stationary part named stator, that comprises permanent magnets and windings (long coils of copper wire) and a moving part named rotor. The heat

losses that occur in the motor can be divided according to the mechanism and component where it happens[50]. So, in the motor we have:

- Iron losses, in stator and rotor laminations;
- Copper losses, in the winding;
- Mechanical losses, due to the resulting friction between solid components;
- Magnet losses, usually the magnets in the rotor;
- Stray losses, considered as the remaining portion of the total losses, in other words, the remaining losses that weren't considered in the previous losses.

2.3.2. Motor Thermal Management System

MTMS is a cooling system that is used to keep the operating temperature of the engines within certain limits, at which the performance and stability of those engines are not affected. One MTMS should be idealized at the beginning of the motor design, because the motor power, efficiency and size are directly connected to the heat dissipation capacity.

These strategies can be divided into two main groups, convection cooling and heat conduction enhancement. In convection cooling, both air cooling and liquid cooling, when applied to the stator, rotor and winding, are perfectly capable of meeting the cooling requirements of different motors. On the other hand, heat conduction enhancement can be made by changing previous materials and components from others with higher thermal conductivity. Moreover, a combination of these two different strategies can also be made for cooling improvement[50].

Even though rotor cooling is important, the cooling strategies applied are still very limited, since it's still a bit of an unexplored subject. So, in the remaining of this subchapter, only the cooling strategies applied to the stator and winding will be addressed (Figure 2.22)

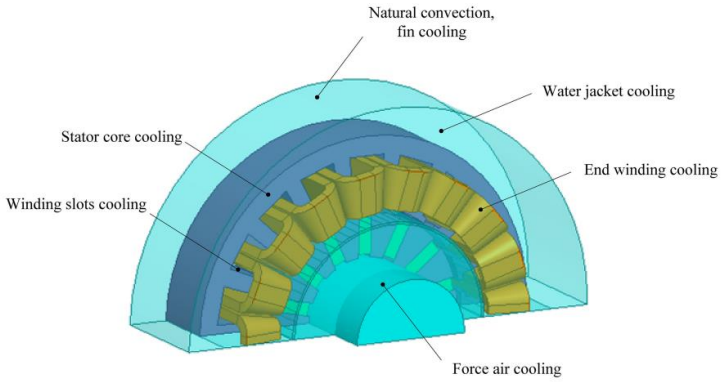

Figure 2.22 - Cooling strategies depending on cooling locations[51]

2.3.2.1. Stator Cooling Strategies

- **Air cooling strategies**

As with the BTMS, air cooling applied to motors is a simple method. It can be made by natural or forced convection and is usually used in low heat density motors. Generally, natural convection is applied to the surface of the motor, while forced convection is better suited for cooling inside the motor. Overall, air cooling is applied to motors with low heat density, as a result of its weak thermodynamic properties, as already mentioned in the BTMS subchapter. Normally, the motor housing possesses fins to increase the heat transfer area [52]. Even though they increase the heat transfer, raising the fins number will also sum more weight and volume. So, it's of great importance to know how the fins geometries, dimensions and number can improve cooling performance. Ulbrich et al.[53] analyze the cooling performance of a few case studies and found out that the housings with 9 fins are better than the ones with 6-8 fins, but from 10 onward the improvement starts to be negligible. Another parameter that improves heat dissipation, concluded from this study, is the increase of the hydraulic diameters[1]. Kuria et al.[54],[55] evaluated 3 different housing geometries and realized that by introducing fins and increasing their depth, the end winding temperature can be reduced up to 15% but the fins orientation does not cause any effect in the end winding temperature.

Inside the motor, air flow and heat transfer are more critical subjects. This is due to the compact internal space, causing the air flow to dominate the heat[56]. Usually, fans are used for this purpose, more specifically axial, centrifugal and piezoelectric fans[57],[58]. They pull the air to the inner path of the motor to cool the components inside. This creates a need to carefully select and optimize the fans and inner air path geometries, since they have great influence in the heat transfer performance of the air flow and in the pressure drop. Kim et al.[59] suggested that direct flow scenario would have better performances than increasing the flow rate. Also, by optimizing some inlet parameters, like location and length, and the groove threshold, the motor performance had an increase of 24.3%. Nakahama et al.[60] changed the air flow path by split it into a double path. This allowed the reduction of the stator temperature and on the other hand reduced the size of the motor.

[1] Geometric parameter for Interior Forced Convection, depending on the cross section geometry.

- **Liquid Jacket Cooling strategy**

This heat dissipation method consists of circulating a liquid coolant, normally water, through a spiral or axial path inside a motor jacket. This dissipation is mainly done by heat convection transfer in the jacket by the liquid[61]. It can be seen as a cylindrical cold plate, since the heat transfer principle is the same. The configuration and the number of cooling paths and the flow rate should be evaluated, since they are the ones that will define the cooling performance just like the pressure drop between the inlet and the outlet. Experiments were made to understand the importance of this strategy. For example, Rehman et al.[62] understood that the maximum temperature of the stator decreased with the increasing of the passages number from 4 to 8; from 8, the increase in the number of passages do not bring significant improvements. Also, they conclude that the increase of the flow rate was more effective on improving the cooling performance. Satrustegui et al.[63] compared different water jackets designs and concluded that the axial jacket had the biggest pressure drop compared to the spiral ones.

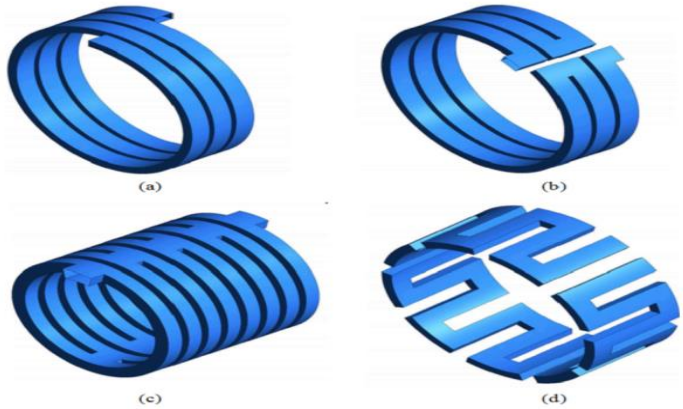

Figure 2.23 - Different configurations of water jackets: (a) spiral; (b) U-shaped; (c) U-shaped (bifurcated); (d) axial[63]

Also, Wu et al.[64] analyzed two different jacket channels, one was smooth and the other was twisted. They saw that the heat transfer coefficient of the twisted one increased, due to the change in the flow characteristics of the water. Also, they realize that the jacket with the twisted channel substantially improved the heat transfer uniformity.

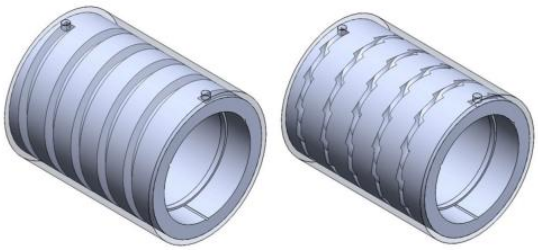

Figure 2.24 - water jacket with spiral coolant channel: without twist (left) with twist (right)[64]

Li et al.[65] said that the increase of the channel width results in a better heat dissipation capacity. On the other hand, the height had a great influence on the pressure distribution instead and not on the temperature. In spite of what has been mentioned before, water is not the only coolant used on experiments. For example, Deriszadeh et al.[66] used water/ethylene glycol and concluded that the increase of the ethylene glycol concentration would lead to an increase of the heat transfer coefficient, because ratio of the density to the viscosity decreases, therefor velocity increases. The optimal transfer rate was achieved at a volume fraction of ethylene glycol to water of 60:40. Yang et al.[67] made an experiment on an oil jacket cooling and concluded that with the increase of the height and the decrease in the width of the channel, the cooling performance would be better, but would lead to a higher pressure drop.

2.3.2.2. Winding Cooling Strategies

Most of the heat generated by electric motors occurs in the winding. This results in a better cooling efficiency compared to the stator cooling strategies[68]. Different cooling strategies are needed according to the winding location. The winding can be divided in slot winding and end winding.

- **Slot winding cooling strategies**

The slot winding considers the parts of the windings inside the stator slots. Even though the slots are a limited space zone, which makes them the worst heat transfer environment, there are a few capable cooling strategies. One of these methods consists in dissipating the heat generated in the windings inside the slots by incorporating cooling channels[69]. It consists in embedding the cooling channels along with the windings inside the slot. Following this strategy, Lindh et al.[70] tested the insertion of cooling ducts in the

slot winding of a permanent magnet motor, and concluded that the cooling capacity was extremely promising, with the average temperatures of motor windings only reaching 77ºC. Reinap et al.[71] also confirmed that the cooling of the slot windings substantially decreased the temperature of the motor. Still, Xu et al.[72] guaranteed that the implementation of cooling channels within the stator was critical to cool the motor. They also implied that using multiple channels evenly distributed through the slot would improve the cooling performance of the windings. By placing 3 cooling ducts within the slot winding, they realized that the temperature decreased by more than 50%. At last, Tuysuzet al.[73] studied the use of axial ducts in the slot windings and concluded that it provided a better cooling capability, compared to the water jacket cooling under the same flow rate. One other possible layout is considered by placing the channels at the top of the slot. To inquire this, Schiefer et al.[74] placed cooling channels at the top of the slots and saw that it had a huge impact in the temperature of the slot winding reducing it from 223.5ºC to 80ºC. The other method is based on the fact that some windings are made of hollow conductors, allowing the winding to provide cooling paths for the coolant, taking back the necessity of considering the previous method. To support this, Alexandrova et al.[75] analyzed a motor with rectangular shape hollow windings, with the coolant(oil) cooling from the bottom of the inner winding to the outer winding, and the results showed that 2.9 out of 3kW were dissipated. With the same goal, Chen et al.[76] idealized and posteriorly tested the cooling for a hollow conductor winding. The outcome indicated that 86.8% of the heat present in the conductor was successfully dissipated through forced convection.

In summary, slot winding cooling is more efficient than stator liquid jacket cooling, due to the fact that windings are the main heat source of the motor. It also increases the output of the motor and can deal with higher current density values. By comparing the two slot winding cooling methods, the hollow conductor's hypothesis provides a more close and efficient cooling[77]. Also, cooling channels scenario brings huge barriers to its implementation. The dimensions of cooling channels need to be very small, because of the slots limited space, which brings a considerable pressure drop of the flow. This results in an increase of power and size of the pump that drives the liquid coolant. The materials used to build the channels are also another limitation. Materials that can increase magnetic losses and safety problems are not recommended; plastics and ceramics aren´t a good option, either, because of their low thermal properties.

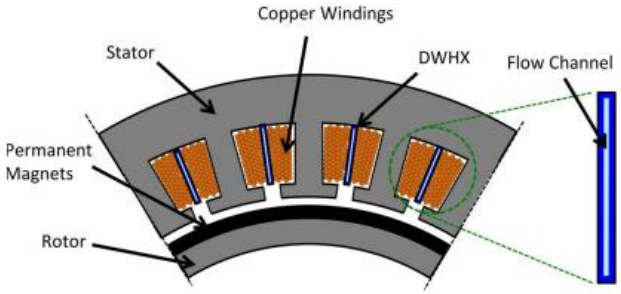

Figure 2.25 - Cooling channels inside the slot method[69]

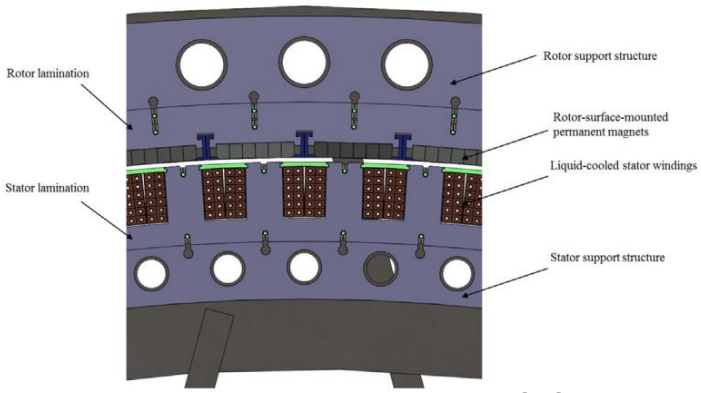

Figure 2.26 - Hollow conductor method[75]

- **End winding cooling strategies**

In typical liquid cooled motors, the biggest temperature spot is encountered in the end winding, caused by the high thermal resistance between the coils and the cooling agent, making the cooling of this zone very important. In fact, and since the end windings are exposed to enormous temperatures, a failure in the insulation system may occur.

The first method consists of the principle of direct liquid cooling strategies to cool the end winding, due to its high heat transfer properties. To support this method, Madonna et al.[78],[79] dropped the end winding temperature, from 172ºC to 130ºC, by applying a cooling pipe passing through the end windings. Also, Marcolini et al.[80] concluded that opting for the oil cooling of the end winding would dissipate 3.3 times more heat, when compared to water jacket cooling.

Another potential cooling method is the jet impingement and spray cooling. Jet impingement can produce huge temperature gradients within the surface, as a result of the large concentration of heat removal in the impingement zone. These gradients are harmful to components, in this case windings, that are sensitive to temperature. This can be solved

by using multiple jets, but by doing this, the interference of consecutive jets tends to difficult the flow of the coolant and create flow instabilities in the cooling module[81]. On this basis, Davin et al.[82] compared the use of lubricating oil under different nozzle configurations and flow patterns. It suggested that even with the smaller quantity of oil, the end winding temperature decreased a lot, and the dissipation capacity grew by 2.5-5 times. Also, a higher flow rate is suggested to improve the winding cooling.

Spray cooling uses the impulse of the liquid emitted through the nozzle to induce the rupture into thin droplets that collide separately with the hot surface. This rupture increases the liquid ratio surface area/volume and promotes a better heat removal distribution along the surface. Vapor can be easily removed, permitting a more effective contact between the droplets and the surface[81]. Studies were conducted to evaluate the importance of this strategy. Li et al.[83] decided to spray oil to the end winding through holes in the end cover and it decreased the temperature of the end winding by 20% and took 30%-60% less time to reach steady state. Liu et al.[84] studied an oil spray cooling with hairpin windings under different parameters and realized that the temperature uniformity increased with a higher oil flow rate and with a higher number of nozzles.

In conclusion, the use of liquid cooling strategies can really reduce the temperature of the end winding. More efficient cooling strategies for the end winding are possible, because there is more space available for cooling them than for cooling slot winding. But end winding cooling also has limitations, like when itis applied to big diameter motors[85], as the cooling in the middle might not be sufficient or due to the annular form of the end winding, which makes it difficult to reach good temperature uniformity.

3. Case Study Cooling System

In this chapter, we start by doing a brief introduction to the vehicle and the designed cooling system. After that, we focus on the critical scenario (firefighting), the different approaches and assumptions used to calculate the different variables needed, in each component.

3.1. The Vehicle

In this subchapter, the E-Forest project vehicle is presented, in which the cooling system will be implemented, introducing the vehicle itself and the components who need to be cooled. The vehicle can be seen in the following Figure (Figure 3.1), where we can visualize the exterior structure of the vehicle with the arm used for forest management and the “hose” for firefighting situation, coupled to a 1000L reservoir.

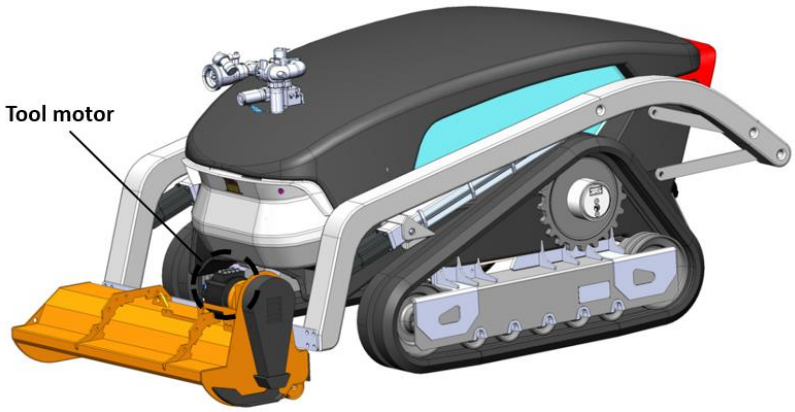

Figure 3.1 - Image of the autonomous vehicle with reference to the tool motor

The vehicle is powered by battery modules that will supply three electric motors and the electronics. Two of those motors, which are identical, serve for locomotion and the other is built in the tool arm for forest management, as can be seen in Figure 3.1. The following figure (Figure 3.2) show the interior from the perspective of the previous figure, being possible to observe the electronics and the space below for the battery pack (orange box).

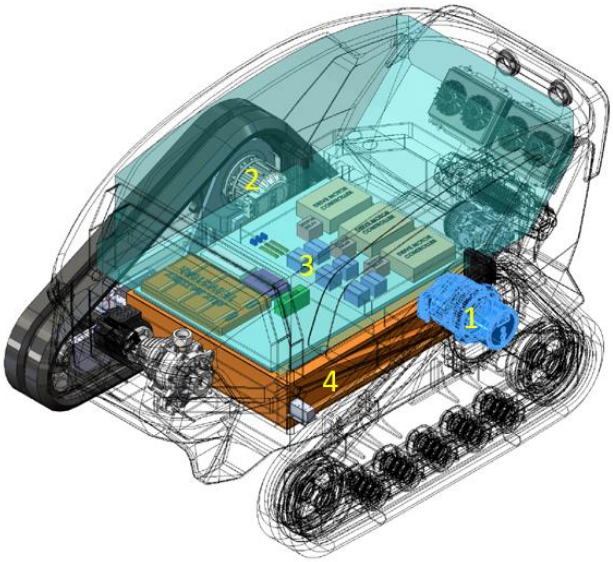

Figure 3.2 - Image of the interior of the autonomous vehicle with reference to the traction motors (1 and 2), electronics (3) and box to the battery pack (4)

Summing up, the components that need to be cooled in this autonomous vehicle are the three motors, the battery pack and the electronics. Important basic information, about these components, that will be obtained and used in chapter 4, can be seen in the following table.

Item	Dissipated Heat /un [W]	Total Dissipated Heat [W]	Tmax operation (ºC)
Batteries	30,7	5500	55
Tool motor	1000	1000	55[2]
Traction motor	1605	3210	100[3]
Electronics	-	625	70

Table 2 - Cooled components data/info

3.2. Cooling System Cycle and Strategies Selected

After evaluating the different existing cooling strategies, the cooling system designed for this case can be seen in the following figure (Figure 3.3).

[2] Value based on the consultation of engines of the same type
[3] Value based on the consultation of engines of the same type

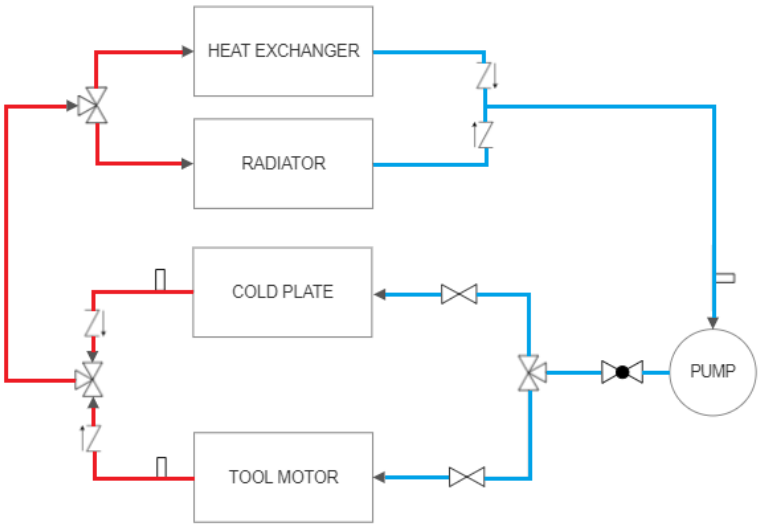

Figure 3.3 - Designed cooling system; Red line - hot fluid, Blue line - Cold fluid

As shown, a radiator liquid cooling system was chosen, with the particularity of an additional heat exchanger, making it a kind of secondary loop liquid system. In addition to these, the system includes other main components, which are the circulation pump, and the cooling strategies for each of the robot components that needed to be cooled. The cooling strategy adopted for the battery pack and the electronics was the cold-plate, sandwiched between them, because liquids are much more efficient when compared to air and also because of the restricted space limitations. About the traction motors, the cooling strategy selected was air-cooling with the help of fans, applying air in the surface of the motors. This system is isolated from the main cooling system. As mentioned earlier, the motor of the tool has an inbuilt cooling system, so there was no need to select another.

This system was designed to fulfill both forest management and firefighting scenarios. In case of forest management, since the ambient air temperature is lower than the working fluid, the pump drives the water to the components, absorbing the heat, and it finally reaches the radiator to dissipate the heat to the ambient air.

When the robot is in firefighting situation, since the ambient air temperature is higher than the working fluid, the radiator becomes insufficient, hence the necessity of a heat exchanger placed inside the water tank with a lower temperature compared to the working fluid. The starting point for building the system was that the water, cooled by both radiator and heat exchanger, depending on the situation, and supplied to the cold-plate and arm motor, should be at a temperature of 30ºC.

3.3. Cold-plate

For this component, a few companies were approached to inquire the viability of the cold-plate, under the case study scenario. The following requirements were defined:

- Double-side Cold-plate maximum dimensions: 810 x 1150 x 25mm;
- Heat to be dissipated, $Q_{cold\ plate}$;
- Maximum temperature of the battery pack (Figure 3.4) and electronics: 55ºC;
- Inlet water temperature of 30ºC;
- Maximum temperature difference between battery modules should never be higher than 5ºC.

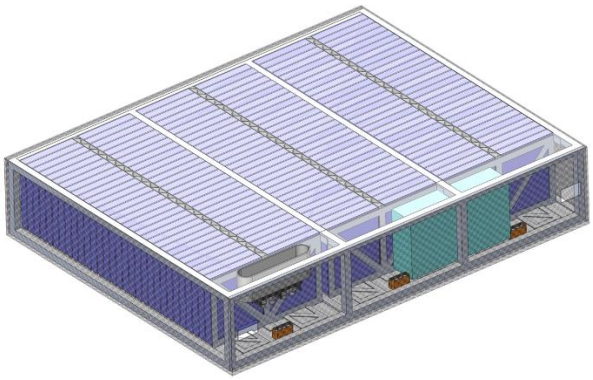

Figure 3.4 - Image of the battery pack

3.4. Traction Motors

The traction motors (Figure 3.5) are basically horizontal cylindrical shape motors that were designed specifically to be cooled by air, so the main goal here is to determine the air velocity needed to attend the heat dissipation requirements, since we are under a exterior forced convection scenario. Also, it should be mentioned that all the fluid properties that appear in the equations are evaluated at a medium temperature between surface and fluid temperatures.

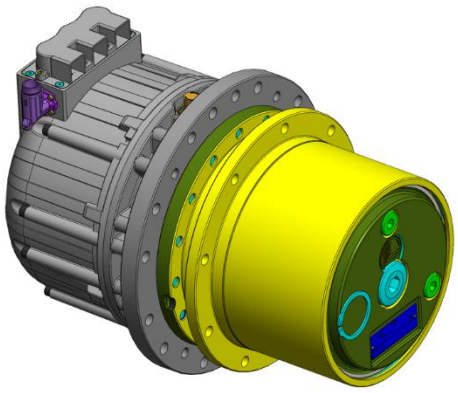

Figure 3.5 - Image of one traction motor

3.5. Tool Motor

In this case, since the tool motor (Figure 3.6) has an inbuilt cooling system, it only requires to be plugged in the cooling system of the vehicle, so the flow rate has to be determined. The motor case possesses two holes (inlet and outlet) for this purpose.

Figure 3.6 - Image of the tool motor[86]

3.6. Heat Exchanger

In this case, Natural convection and Interior forced convection are present.

In order to be able to determine the length, a few initial assumptions were made:

- Water tank initial temperature of 20ºC and at steady state;
- Water pipe outlet temperature of 30ºC;
- Pipe diameter of 1 inch in the entire cooling system;

- Thin pipe walls, which leads to $R_{t_{wall}} \approx 0$ and $A_i \approx A_e = A$ and consequently the surface temperature of the pipes will be the same of the circulating water inside.

3.7. Radiator

For the radiator, a few potential suppliers were contacted.

The following requirements were set:

- Dissipated heat, $Q_{total} = Q_{cold\ plate} + Q_{tool\ motor}$;
- Maximum width of 800mm;
- Maximum height of 315mm;
- Inlet and outlet size of 1 inch;
- Water as working fluid;
- Need of at least 1 DC cooling fan, due to the low speed of the vehicle, which is about 1.6m/s.

3.8. Pump

The function of the pump is to circulate the fluid inside the cooling system. The selection of the pump depends on three factors, pressure losses, fluid flow rate and manometric height.

3.9. Other Components

In addition to all the components mentioned previously in this chapter, other components must be included for the proper functioning of the cooling system.

In this subchapter, types and quantities of the remaining components are exposed, as well as a control system operation proposal, based on the selected components.

3.9.1. Valves

All valves were selected to comply with certain main requirements:

- Dimension of 1 inch;

- Range of operating temperatures;
- Maximum pressure;
- If solenoid valves, power supply: 12V, 24V, 96V (all DC).

- **Check Valves**

These valves oblige the fluid to flow in only one direction to prevent situations where pressure conditions could lead to reversed flows. In this case, 4 check valves will be required. Each one should be placed after the radiator, heat exchanger, cold-plate and arm motor.

- **3-way Valves**

These valves allow the flow cutoff or to even split it two ways. One other type are the thermostatic 3-way valves that permits mixing fluid from 2 different paths. In this case, two 3-way valves will be inserted, one of them being thermostatic. The thermostatic valve will make the link between the outlet tubes of the cold-plate and the arm motor, leading the mixed water to the 3-way valve, that will be linked to the heat exchanger and radiator pipe circuits.

- **2-way flow regulator valves**

These valves will help to control the fluid flow rate in the system. In this case, two 2-way valves will be needed. One of them, number 1, will be placed before the cold-plate and the other, number 2, before the arm motor, so that the circulating fluid flow rate in both components can be controlled.

- **Sectioning Valves**

The function of these valves is to interrupt the fluid flow for possible repairs in the system. In this case, one sectioning valve will be installed after the pump.

3.9.2. Sensors

- **Temperature sensors**

There are many types of temperature sensors, but they all have the same purpose, which is measuring a determined temperature. In this case, 3 temperature sensors will be inserted in the system. One before the pump and each one of the other two at the exit of the cold-plate and arm motor.

3.9.3. Proposed Control System

The system standard scenario will be the radiator circuit. When the outlet temperature of the radiator, measured by the temperature sensor, is higher than 30ºC and the radiator fan is working at full power, a signal will be sent to the 3-way valve linked to the radiator and the heat exchanger and will change the direction of the flow from the radiator pipes to the heat exchanger pipes. When functioning on heat exchanger scenario, when the outlet temperature of the heat exchanger, measured by the temperature sensor, is higher than 30ºC, it should send a signal to turn off all non-vital functions and limit power usage on motors, actuators and electronics, in order to reduce heat output.vAlso, when the outlet temperatures of the cold-plate or the arm motor, measured by the respective temperature sensors, are higher than 33ºC and 50ºC, respectively, a signal will be sent to the 2-way valves to readjust the fluid flow rate and pump flow. This control system should be able to respond to the needs of the cooling system. In the following figure (Figure 3.7), a scheme of the cooling circuit with these components can be seen.

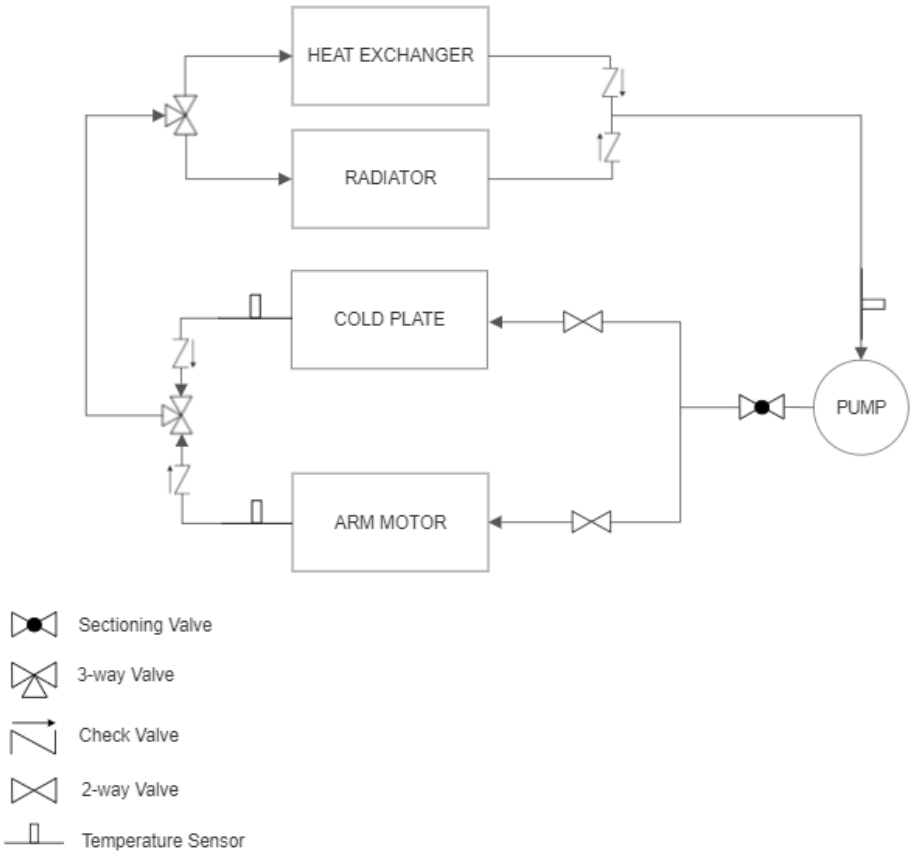

Figure 3.7 - Cooling system schematic with valves and sensors for proposed control system

4. Results and Selection of Components

In this chapter, the methodologies and results obtained from the approaches in the previous chapter are presented.

4.1. Cold-Plate

In order to calculate the heat released by the battery pack, the extreme situation of discharging the batteries was considered.

Charge current 1C means that the load will be fully charged in 1 hour with a charge current of 105 A. Discharge current 2C means that the battery will discharge in 0.5h or 30 minutes, but with twice of the cell current, which is 210 A. The cell's internal resistance is 0.7 mΩ. First, the heat dissipated has to be determined. The heat dissipated by the electronics can be seen in ANNEX A and the batteries can be determined by using the following equation (4.1):

$$q_{battery\ pack} = I^2 \times R \quad \textbf{(4.1)}$$

Where I is the current and R the resistance of the battery cell (ANNEX A).

Table 3 shows the result of the heat dissipated by the battery pack.

$I(A)$	$R(\Omega)$	$Q_{1\ cell}(W)$	N_{cells}	$q_{battery\ pack}(W)$
210	0,0007	30,8	180	5544

Table 3 - Results for the heat dissipated in the battery pack

Resuming, the total heat that needs to be dissipated in worst case scenario (battery pack and electronics (ANNEX A)) is around 6200W.

It should be noted that, in nominal functioning, the batteries deliver about 100A, which results in a dissipated heat of 2270W.

The response from the cold-plate suppliers was generally positive. One of them even performed a CFD analysis, which was then provided.

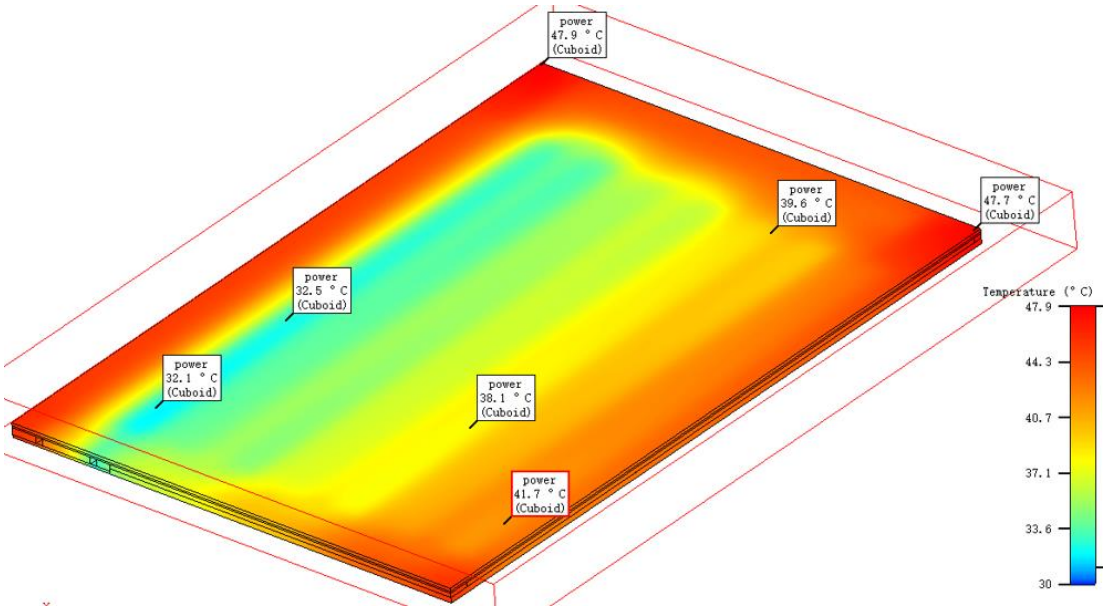

Figure 4.1 - Cold-plate CFD analysis (Temperature), provided by Regis Heat sink Technology Co., Ltd.

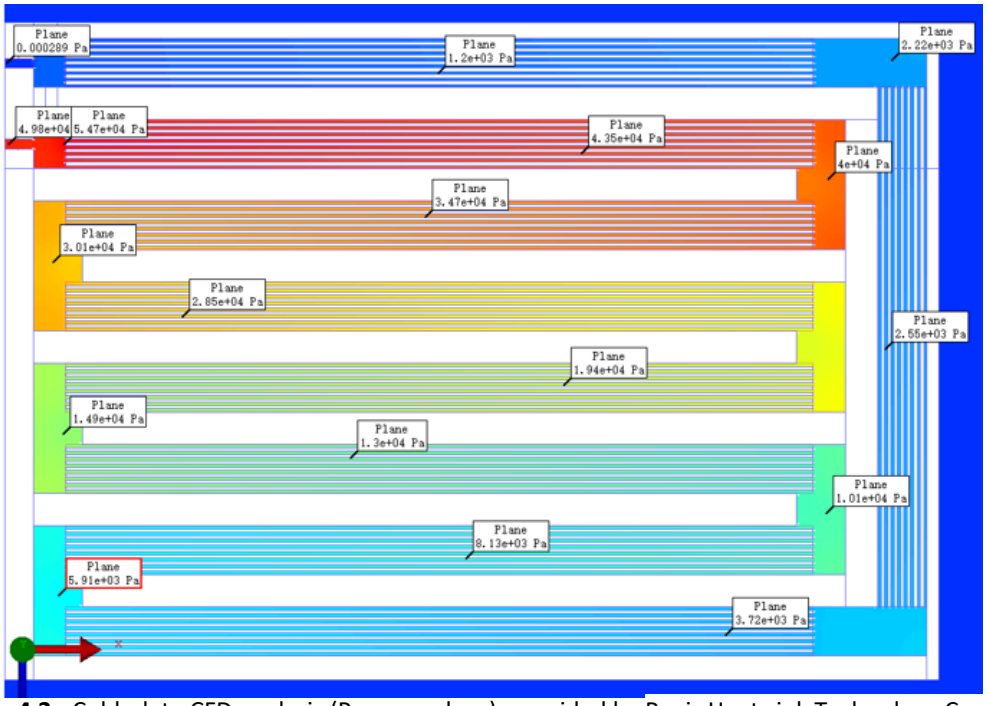

Figure 4.2 - Cold-plate CFD analysis (Pressure drop), provided by Regis Heat sink Technology Co., Ltd.

The CFD analysis (Figure 4.1, Figure 4.2), provided by Regis Heat sink Technology Co., Ltd., shows that the cold-plate that managed to keep the temperature of the battery pack under 48ºC, which is lower than the maximum 55ºC, had the following dimensions, 810x1150x25mm. This was achieved through a water flow rate of $1.8m^3/h$ entering the cold-plate at 30ºC. Also, the pressure drop registered was of $54700\ Pa$. The CFD analysis

that was performed wasn't the most accurate, since they considered 7500W for the heat dissipated instead of 6200W and the analysis was made for a one side cold plate. Regardless of that, since the heat dissipation considered was higher than the real one and the electronics side corresponds only to 700W of the 6200W, it was decided to carry on with these results later on. The water outlet temperature was not mentioned in the CFD analysis, so it had to be determined. By using the equation (4.8) and the following data, present in Table 4, the value of temperature was determined. Fluid properties were determined at a medium temperature between the inlet water temperature and the maximum temperature of the battery pack. Water properties were extracted at a medium temperature of 31.5ºC (approximately 30ºC).

$\dot{Q}(m^3/s)$	$q(W)$	$c_p(J/kg.K)$	$\rho(kg/m^3)$	$T_{in}(ºC)$	$T_{out}(ºC)$
5,085E-04	6200	4178	996	30	32,92

Table 4 - Results for cold-plate outlet temperature

4.2. Traction Motors

First, heat dissipated can be obtained through:

$$Q_{traction\ motor} = P_{in} \times (1 - \eta) \tag{4.2}$$

Where P is the power input and η the efficiency of the traction motor (ANNEX A). The results for heat dissipated by the thinning arm motor can be seen in Table 5.

$P_{in}(W)$	$\eta(\%)$	$Q(W)$
10700	85	1605

Table 5 - Results for the heat dissipated in the traction motor

By using the following data and equations, the obtained results are shown in Table 6. Air properties were extracted at a medium temperature of 75ºC =348.15K (approximately 350K). Entry data:

- Motor geometry: cylinder with a diameter of 0.23m and length of 0.147m;
- Heat dissipated: $Q = 1605W$;
- Motor surface temperature: $T_{sup} = 120ºC$;
- Air temperature: $T_{\infty} = 30ºC$.

The air heat transfer coefficient,h,has to be obtained, through Newton law:

$$q_{traction\ motor} = h \times A_{sup} \times (T_{sup} - T_{\infty}) \quad \textbf{(4.3)}$$

Where Q is the heat dissipated, A the surface area and T and T_{∞} are the surface temperature and fluid temperature, respectively.

After this, based on a forced convection scenario, the Nusselt number is calculated:

$$Nu = \frac{h \times D}{k_f} \quad \textbf{(4.4)}$$

Where D is the diameter of the motor and k_f is thermal conductivity of the fluid.

Now, the Reynolds number (Re) can be determined. Based on the surface geometry, the Churchill-Bernstein correlation (4.5) as selected, mainly because it is the one with the largest range of values.

$$\overline{Nu_D} = 0{,}3 + \frac{0{,}62 Re_D^{1/2} Pr^{1/3}}{\left[1 + \left(\frac{0{,}4}{Pr}\right)^{2/3}\right]^{1/4}} \left[1 + \left(\frac{Re_D}{282000}\right)^{5/8}\right]^{4/5} \quad \textbf{(4.5)}$$

Where Pr is the Prandtl number of the fluid.

Finally, air velocity, u_{∞}, is determined through the following equation (4.6):

$$Re = \frac{u_{\infty} \times D}{\nu} \quad \textbf{(4.6)}$$

Where ν is the kinematic viscosity of the fluid.

The results for these equations are presented in Table 6.

$P_s(m)$	0,723	$k_f(W/m.K)$	0,03
$A_{sup}(m^2)$	0,106	Pr	0,7
$h(W/m^2.K)$	167,895	Nu	1287
$\alpha(m^2/s)$	2,990E-05	Re	1,059E+06
$\nu(m^2/s)$	2,092E-05	$u_{\infty}(m/s)$	96,3

Table 6 - Results of air speed required for traction motors

The heat transfer coefficient is inside the range values for typical air forced convection values, but air velocity required is completely unrealistic, so the motors manufacturers were contacted in order to better understand the motors characteristics, since the motors had been designed to be able to be cooled by air. So far there has been no response from them, so a possible hypothesis to solve this problem is the increase of surface area with fins. A graphic showing approximately how the addition of area to the motor surface area influence the air velocity required is shown below.

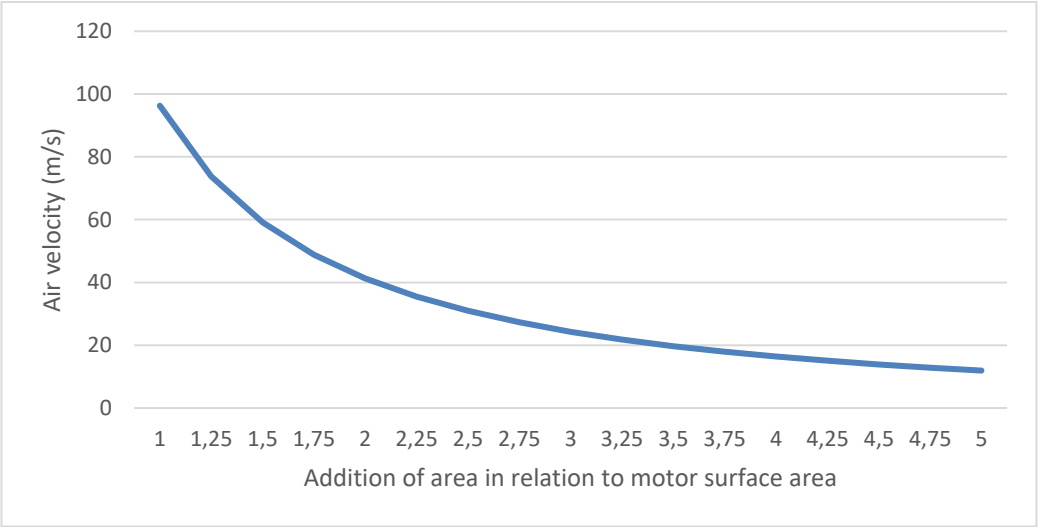

Figure 4.3 - Variation of air flow required with the addition of surface area in relation with the base motor area

As the graphic shows, as the surface area increases, the air velocity needed decreases. But we can also see, in this situation, that, from a certain point, the addition of area won't bring many benefits, since the curve tends to stabilize. A careful analysis has to be done, since the increment of area will also increase the motor weight.

4.3. Tool Motor

The heat dissipated can be determined by using equation (4.2), where P_{in} is the power input and η the efficiency of the tool motor (ANNEX A). The results for heat dissipated by the thinning arm motor can be seen in Table 7.

$P_{in}(W)$	$\eta(\%)$	$Q(W)$
10419,78	90,3	969

Table 7 - Results for the heat dissipated in the tool motor

Now, the water volumetric flow rate, $\dot{Q}$, is obtained through:

$$q_{tool\ motor} = \dot{Q} \times c_p \times \rho \times \Delta T \quad \textbf{(4.7)}$$

Where C_p is the water specific heat, ρ is the water density and ΔT is the difference between the initial and final temperature of the circulation fluid.

Assuming that the inlet water temperature is 30ºC, and should achieve an outlet temperature of 50ºC (a bit lower than the desired motor surface temperature of 55ºC), by dissipating approximately 1000W (oversized value relatively to the one in Table 7), we can finalize the calculus (Table 8). Water properties were extracted at a medium temperature of 40ºC.

$T_{in}(ºC)$	$T_{out}(ºC)$	$q(W)$	$c_p(J/kg.K)$	$\rho(kg/m^3)$	$\dot{Q}(L/min)$
30	50	1000	4179	992,1	0,724

Table 8 - Results for water flow rate of tool motor

The water flow required is almost negligible when compared to the flow required by the cold-plate.

4.4. Heat Exchanger

Now that the outlet temperatures and water flow rate for both cold-plate and thinning arm motor are known, the total water flow rate and temperature can be determined.

For the total water flow rate, the flows in each component need to be summed:

$$\dot{Q}_{total} = \dot{Q}_{cold\ plate} + \dot{Q}_{tool\ motor} \quad \textbf{(4.8)}$$

For the temperature of the total water flow rate, considering an adiabatic system, we make a temperature balance:

$$\dot{Q}_{total} \times T_{total} = \dot{Q}_{cold\ plate} \times T_{out,cold\ plate} + \dot{Q}_{tool\ motor} \times T_{out,tool\ motor} \quad \textbf{(4.9)}$$

Now that $\dot{Q}_{total}$ and T_{total} (inlet temperature in heat exchanger) are known, the pipe length necessary to dissipate the required heat can be obtained. Since this is a situation of natural convection outside the tube, the first thing to do is determine heat transfer coefficient of natural convection.

- **Natural convection**

First, the Rayleigh number,Ra_D, has to be calculated:

$$Ra_D = \frac{g \times \beta \times (T - T_\infty) \times D^3}{v \times \alpha} \quad \textbf{(4.10)}$$

Where g is the gravity, β is the volumetric expansion coefficient of the fluid, T is the temperature of the surface that will be considered equal to the fluid temperature inside the tube, T_∞ is the temperature of the fluid, D is the diameter of the tube,v is the kinematic viscosity of the fluid and α is the thermal diffusivity of the fluid.

After obtaining Rayleigh number, having in consideration the geometry of the surface area, the Nusselt number, $\overline{Nu_D}$, must be determined:

$$\overline{Nu_D} = C \times Ra_D^m \quad \textbf{(4.11)}$$

Where C and m are constants and their values depend on the Rayleigh number.

Finally, the convection coefficient, h_e, is given by:

$$h = \frac{Nu_D \times k_f}{D} \quad \textbf{(4.12)}$$

Where k_f is the thermal conductivity of the fluid.

It is important to mention that all fluid properties are extracted at a medium temperature between the temperature of the deposit water and the pipe surface.

Table 9 will present the values for the natural convection process (water properties extracted at a medium temperature of 26.5ºC (approximately 25ºC)).

$g(m/s^2)$	9,81	Pr	6,140
$\beta(1/K)$	2,47E-04	Ra	3,81E+06
$T_{sup}(ºC)$	33,3	C	0,480
$T_{\infty}(ºC)$	20	m	0,250
$D(m)$	0,025	Nu	21,207
$\nu(m^2/s)$	8,94E-07	$k_f(W/m.K)$	0,607
$\alpha(m^2/s)$	1,456E-07	$h(W/m^2.K)$	517,1

Table 9 - Results for water heat transfer coefficient (Heat Exchanger)

Since area is the only variable unknown, the Newton law can be used to determine it:

$$q_{total} = h \times A \times (T - T_{\infty}) \quad \textbf{(4.13)}$$

Where Q represents the heat dissipated, A the surface area, T the surface temperature and T_{∞} the water tank temperature.

Now that everything is known to determine the required surface area, having the diameter of the pipes, D, the pipe length, L, necessary can be obtained. Considering, the surface area of a cylinder, a rectangle, where $W = Perimeter_{circle}$:

$$A = \pi \times D \times L \quad \textbf{(4.14)}$$

Table 10 shows the values for the tube surface area and length.

$h(W/m^2.K)$	517,1	$A(m^2)$	1,045
q_{total}	7200	$W(m)$	0,079
$T_{sup}(ºC)$	33,3	$L(m)$	13,3
$T_{\infty}(ºC)$	20		

Table 10 - Results for tube surface area and length (Heat Exchanger)

A safety factor of approximately 1.45 was assumed for the length of the heat exchanger. This led to a length of approximately 19.365m.

- **Interior forced convection**

Associated with the length, pressure losses, ΔP, can be calculated:

$$\Delta P = f \times \left(\frac{L}{D}\right) \times \frac{1}{2} \times \rho \times u_m^2 \quad \textbf{(4.15)}$$

Where f is the friction factor, ρ is the density of the water inside the tube and u_m the medium velocity of the water inside the tube.

To determine the friction factor, first the Reynolds number, Re_{D_h}, associated with the interior forced convection must be obtained:

$$Re_{D_h} = \frac{4 \times \dot{Q}}{\nu \times P_s} \quad \textbf{(4.16)}$$

Where $\dot{Q}$ is the water volumetric flow rate of the fluid, P_s is the section perimeter and ν is the kinematic viscosity of the fluid.

The Reynolds number allows knowing the regime of the flow. In this case, since the Reynolds number is higher than 10^4, a fully developed turbulent flow is guaranteed.

In a turbulent regime, Pethukov defined the friction factor as:

$$f = (0.79 \times \ln(Re_D) - 1.64)^{-2} \quad \textbf{(4.17)}$$

Note that all fluid properties needed for the calculus are determined at a medium temperature between the inlet and outlet temperature of the pipe water.

Table 11 presents the values for the pressure drop (water properties extracted at a medium temperature of 31.5ºC (approximately 30ºC)).

$\dot{Q}(m^3/s)$	5,121E-04	$L(m)$	19,365
$\nu(m^2/s)$	8,012E-07	$D(m)$	0,025
$P_s(m)$	0,079	$\rho(kg/m^3)$	996
Re	32550	$u_m(m/s)$	1,043
f	0,023	$\Delta P(Pa)$	9729

Table 11 - Results for Pressure Losses inside the tube (Heat Exchanger)

The heat transfer coefficient is inside the range values for typical water natural convection values. A good solution for the tube material is copper, due to its high thermal conductivity.

4.5. Radiator

After contacting some companies with the necessary requirements, the company Shanghai Shenglin M&E Technology Co.,Ltd, answered affirmatively. In talks with them, a microchannel radiator was decided. It was also decided, the use of two fans (Figure 4.4), which specifications are in ANNEX A, to increase the heat dissipation.

Figure 4.4 - Fans selected for the radiator

4.6. Pump

Taking into account the pressure drop values of the entire system, the ΔP_{total} can be obtained. Since the pressure losses in the arm motor and in the radiator are unavailable, both of them were considered an approximate value (50000Pa) of the cold-plate losses. So far, the known pressure losses are available in Table 12.

ΔP_{valves}(Pa)	26470
$\Delta P_{cold\ plate}$(Pa)	54700
$\Delta P_{radiator}$(Pa)	50000
$\Delta P_{heat\ exchanger}$(Pa)	9729
$\Delta P_{tool\ motor}$(Pa)	50000

Table 12 - Known pressure losses of the entire cooling system

To determine the losses in the pipelines, same steps and values of heat exchanger interior forced convection section will be used. The only thing that differs is the pipeline length that has to be estimated. The pipeline length considered to determine the corresponding pressure losses won't include the pipe concerning the arm motor, since the

corresponding water flow is almost inexistent compared to the one in the cold-plate. The estimated length for the pipeline can be seen in the following figure and in Table 13.

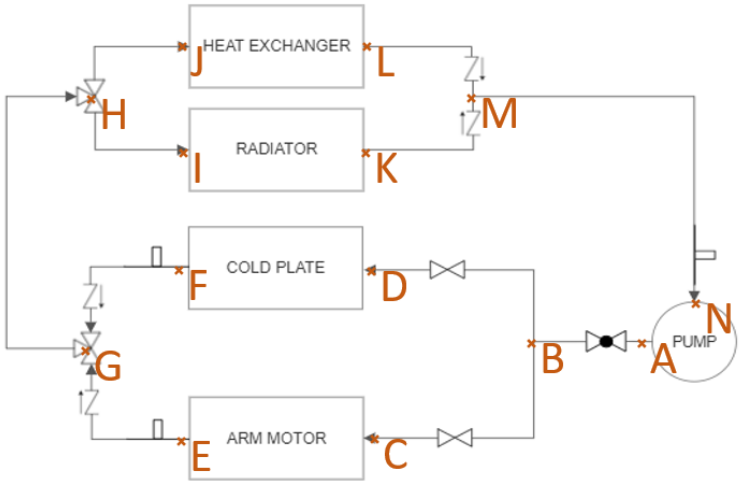

Figure 4.5 - Pipe designations for length calculation

Pipe	Type	Diameter	Length [mm]	N elbows	N Tderiv.	Temperature
AB	PVC	1"	300	2	1	cold
BC	PVC	1"	1500	2	0	cold
BD	PVC	1"	140	0	0	cold
EG	PVC	1"	1500	2	0	hot
FG	PVC	1"	140	0	0	hot
GH	PVC	1"	300	2	1	hot
HI	PVC	1"	900	3	0	hot
HJ	PVC	1"	500	3	0	hot
JL	Copper	1"	19365	28	0	hot
KM	PVC	1"	200	2	0	cold
LM	PVC	1"	200	2	0	cold
MN	PVC	1"	400	1	0	cold
		Total	25445			

Table 13 - Pipeline length values

The length used for the pressure drop didn't include JL, BC and EG pipes, so the final value was 3080mm (3.08m). Having this in account, by using the same equation(4.15) and values of heat exchanger subchapter (flow rate of the cold-plate is almost equal to the total flow rate) and only changing the length value, an approximate value of $\Delta P_{pipeline}$ can be obtained (Table 14).

$\dot{Q}(m^3/s)$	5,121E-04	$L(m)$	3,08
$\nu(m^2/s)$	8,012E-07	$D(m)$	0,025
$P_s(m)$	0,079	$\rho(kg/m^3)$	996
Re	32550	$u_m(m/s)$	1,043
f	0,023	$\Delta P(Pa)$	1547

Table 14 - Results for pressure drop inside the tube (Pipeline)

Also, it is worth mentioning that, since the heat should not be released by the pipelines, they should have thermal insulation. In this case, PVC (Polyvinyl chloride) was chosen, due to its low thermal conductivity.

The fluid flow rate, $\dot{Q}_{total}$, was determined earlier, missing the calculus of manometric height. The manometric height, H,can be obtained through the following equation (4.18):

$$H = \frac{\Delta P_{total}}{\rho \times g} \quad \textbf{(4.18)}$$

The ΔP_{total} is the sum of the pressure losses in each component and in the pipes as can be seen next:

$$\Delta P_{total} = \Delta P_{cold\ plate} + \Delta P_{tool\ motor} + \Delta P_{rad\ or\ h.e} + \Delta P_{pipeline} + \Delta P_{valves} \quad \textbf{(4.19)}$$

Since the radiator and the heat exchanger won't be working simultaneously, for sizing purposes, $\Delta P_{rad\ or\ h.e}$ is considered the highest pressure drop value among them.

Table 15 shows the value for the manometric height. Water density extracted at a temperature of 30ºC.

$\Delta P_{total}(Pa)$	$\rho(kg/m^3)$	$g(m/s^2)$	$H(m)$
182717	996	9,81	18,7

Table 15 - Results for pump manometric height

Now, that ΔP_{total}, $\dot{Q}_{total}$ and H are known, a pump can be selected, having in consideration that the power supplies available in the vehicle are 12V, 24V and 96V, all DC. Note that ΔP_{valves} is determined in the next subchapter. After some research made to find a proper bomb, it was concluded that for the requirements needed, a single pump couldn't be found. So, the solution found was the HIGH FLOW SYSTEM 12VDC 10.0GPM from

Shurflo (Figure 4.6), which is composed of two pumps. The pump datasheet is available in ANNEX A.

Figure 4.6 - Image of selected pump

4.7. Other Components

4.7.1. Valves

- **Check Valves**

For these valves, the model **3047**60 (Figure 4.7) from Caleffi was selected. The extracted pressure drop values, based on the flow rate and connection dimensions, are:

- $\Delta P_{rad} = 3{,}2kPa = 3200Pa$;
- $\Delta P_{heat\ exchanger} = 3{,}2kPa = 3200Pa$;
- $\Delta P_{arm\ motor} \approx 0Pa$;
- $\Delta P_{cold\ plate} = 3{,}1kPa = 3100Pa$;

The specifications of the product and the hydraulic characteristics can be seen in ANNEX A.

- **3-way Valves**

For these valves, the model VG 3310 LS (Figure 4.7) with thermoelectric ON/OFF actuator from Johnson Controls, was selected and the chosen model for the thermostatic valve was the **5230**60 (Figure 4.7) from Caleffi. The extracted pressure values, based on the flow rate and connection dimensions, are:

- $\Delta P_{3-way} = 4{,}2kPa = 4200Pa$ (Assumed from other 3-way valves; no information available from the manufacturer) ;
- $\Delta P_{thermostatic} = 0{,}08bar = 8000Pa$.

The specifications of the products and the hydraulic characteristics of the thermostatic can be seen in ANNEX A.

- **2-way Valves**

For these valves, the model VG 3210 LS (Figure 4.7) with electric modulating action actuator from Johnson Controls, was selected. Based on the flow rate and connection dimensions, the extracted pressure values are:

- $\Delta P_1 = 0{,}27kPa = 270Pa$ (Assumed from other 2-way valves; no information available from the manufacturer);
- $\Delta P_2 \approx 0Pa$ (Assumed from other 2-way valves; no information available from the manufacturer).

The specifications of the product can be seen in ANNEX A.

- **Sectioning Valves**

The valve selected for this purpose was the **3230**60 (Figure 4.7) from Caleffi. The extracted pressure value, based on the flow rate and connection dimensions, was:

- $\Delta P = 0{,}045bar = 4500Pa.$

The specifications of the product and the hydraulic characteristics can be seen in ANNEX A.

Figure 4.7 - Valves selected: (a)check valve, (b)3-way valve, (c)thermostatic valve, (dd)2-way valve, (e)sectioning valve

4.7.2. Temperature Sensors

The temperature sensors selected were the same. For this purpose, the PTV (Figure 4.8) from ACS control-system was chosen (ANNEX A). It has the advantage of being easily installed, without the need to be incorporated in the pipeline system.

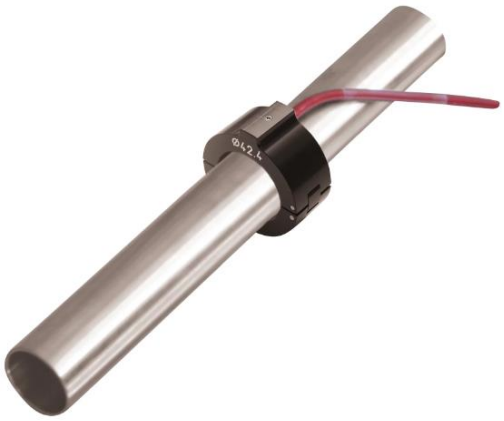

Figure 4.8 - Image of selected temperature sensor

4.8. Implementation of main components

The implementation of the heat exchanger, pump and radiator can be seen in the following figure (Figure 4.9).

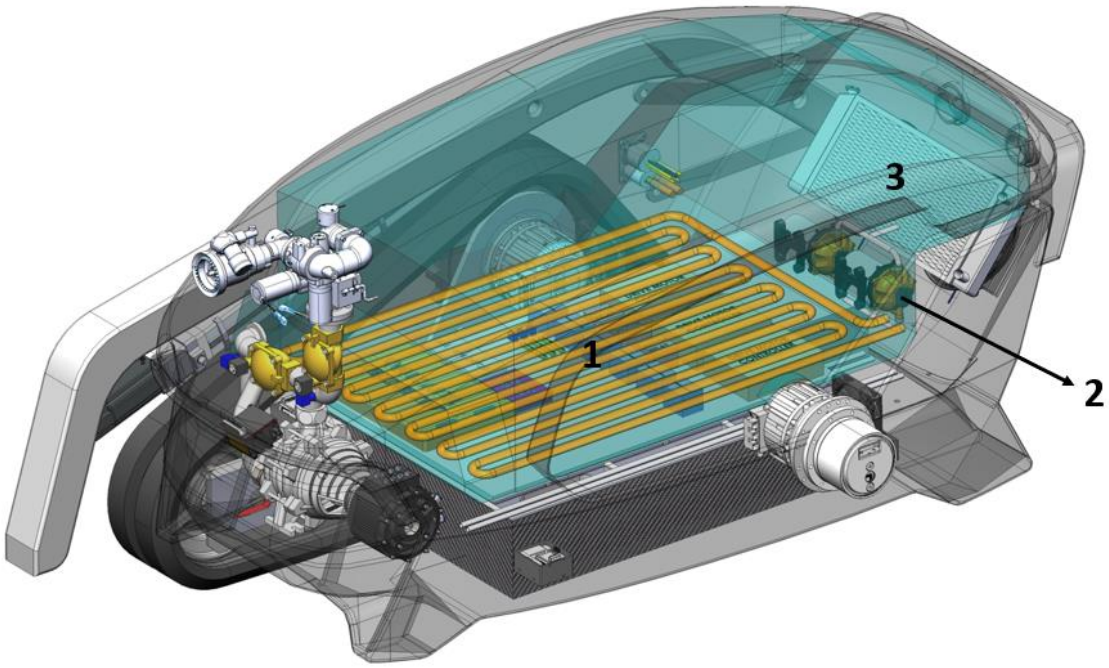

Figure 4.9 - Implementation of heat exchanger(1), pump(2) and radiator(3) in the vehicle

5. Conclusions

The objective of this dissertation's work was building a cooling system for the autonomous vehicle of the E-Forest project, so that it can operate in forest management tasks and firefighting situations. The researched state-of-art allowed a deeper understanding of cooling strategies applied to electric components, allowing a good framework for this project. This research provided the basis and subsequent analysis resulted in the proposed cooling system and to the selection of components. The main difficulty arose around the traction motor cooling results. Unfortunately, it wasn't possible to get a timely response from the motor manufacturers. However, since it was isolated from the main cooling system, it didn't affect the results obtained in other components.

Overall, considering that, the system was designed taking into account the worst case scenarios of the component operation, and conservative safety factors, it is believed that it will perform efficiently under the most extreme conditions. This work and findings can positively contribute to the designing of reliable and robust cooling systems for autonomous vehicles in extreme heat scenarios.

5.1. Future Work

In the future, there are a few things that should be done. The most pressing is to get a response from the traction motors manufacturers and determine the correct air velocity required, so that a proper air cooler (fan) can be chosen. Cold-plate was already defined with the correct requirements, from Regis Heat sink Technology Co., Ltd., but there are no specifications available yet. For a more accurate analysis, the respective CFD analysis, with the right values, should be consulted, to compare results with the previous CFD. Radiator was also defined with the needed requirements, from Shanghai Shenglin M&E Technology Co.,Ltd, but there are no specifications yet. So, the remaining components should be obtained too.

The control system is yet to be designed and should include the following functions:

- If the measured temperature after the radiator is higher than 30ºC, the 3-way valve should change the flow direction to the heat exchanger;

- If the measured temperature after the heat exchanger is higher than 30ºC, it should turn off all non-vital functions and limit power usage on motors, actuators and electronics;
- If the measured outlet temperatures of the cold-plate or the tool motor, are higher than 33ºC and 50ºC respectively, the 2-way valves should readjust the fluid flow rate and pump flow.

After this, in a first stage, with all components and a defined control system software, the system should be tested in laboratory environment.

Finally, if it meets all the requirements under lab environment, the system must be tested and validated in the vehicle prototype in real life scenarios.

REFERENCES

[1] INSTITUTO DA CONSERVAÇÃO DA NATUREZA E DAS FLORESTAS, "8.º RELATÓRIO PROVISÓRIO DE INCÊNDIOS RURAIS," 2022. Accessed: Feb. 01, 2023. [Online]. Available: https://www.icnf.pt/api/file/doc/4e8a66514175d0f7

[2] B. Abraham, "The Roots of Forest Loss and Forest Governance," 2022. Accessed: Feb. 01, 2023. [Online]. Available: https://www.iisd.org/system/files/2022-05/still-one-earth-forests.pdf

[3] F.-N. Robinne, "Impacts of disasters on forests, in particular forest fires," pp. 2–2, 2021, Accessed: Feb. 01, 2023. [Online]. Available: https://www.un.org/esa/forests/wp-content/uploads/2021/08/UNFF16-Bkgd-paper-disasters-forest-fires_052021.pdf

[4] "Firefighting Robotic Vehicle System - Fire Apparatus: Fire trucks, fire engines, emergency vehicles, and firefighting equipment." https://www.fireapparatusmagazine.com/fire-apparatus/firefighting-robotic-vehicle-system/ (accessed Feb. 01, 2023).

[5] "Multiscope Rescue with Hydra - Milrem." https://milremrobotics.com/product/multiscope-rescue-hydra/ (accessed Feb. 01, 2023).

[6] "Multiscope Rescue Hose Cartridge - Milrem." https://milremrobotics.com/product/firehouse-container/ (accessed Feb. 01, 2023).

[7] "SHARK ROBOTS — SHARK ROBOTICS." https://www.shark-robotics.com/shark-robots (accessed Feb. 01, 2023).

[8] "RTE Robot - Rosenbauer." https://www.rosenbauer.com/en/pt/rosenbauer-world/products/equipment/rte-robot (accessed Feb. 10, 2023).

[9] "Wolf R1 tactical response robot by Magirus." https://www.magirusgroup.com/de/en/products/special-vehicles/wolf-r1/ (accessed Feb. 10, 2023).

[10] "Emergency robot for Wildland, structural fire and rescue operations | Dronster." https://www.vallfirest.com/en/dronster-forestry-mulcher/# (accessed Feb. 10, 2023).

[11] "MVF-5 - DOK-ING." https://dok-ing.hr/defence-security/mvf-5/ (accessed Feb. 10, 2023).

[12] V. Etacheri, R. Marom, R. Elazari, G. Salitra, and D. Aurbach, "Challenges in the development of advanced Li-ion batteries: a review," *Energy Environ Sci*, vol. 4, no. 9, pp. 3243–3262, Aug. 2011, doi: 10.1039/C1EE01598B.

[13] A. Greco, D. Cao, X. Jiang, and H. Yang, "A theoretical and computational study of lithium-ion battery thermal management for electric vehicles using heat pipes," *J Power Sources*, vol. 257, pp. 344–355, Jul. 2014, doi: 10.1016/J.JPOWSOUR.2014.02.004.

[14] Q. Wang, J. Sun, and G. Chu, "Lithium Ion Battery Fire and Explosion," 2005.

[15] Z. Y. Jiang, H. B. Li, Z. G. Qu, and J. F. Zhang, "Recent progress in lithium-ion battery thermal management for a wide range of temperature and abuse conditions," *Int J Hydrogen Energy*, vol. 47, no. 15, pp. 9428–9459, Feb. 2022, doi: 10.1016/J.IJHYDENE.2022.01.008.

[16] A. A. Pesaran, “Battery thermal models for hybrid vehicle simulations,” *J Power Sources*, vol. 110, no. 2, pp. 377–382, Aug. 2002, doi: 10.1016/S0378-7753(02)00200-8.
[17] A. A. Pesaran, “Battery Thermal Management in EVs and HEVs: Issues and Solutions Some of the authors of this publication are also working on these related projects: Multi-scale mechanical-electrochemical-thermal coupled modeling framework for lithium-ion battery under mechanical abuse View project”, Accessed: Feb. 01, 2023. [Online]. Available: https://www.researchgate.net/publication/237250969
[18] S. Arora, “Selection of thermal management system for modular battery packs of electric vehicles: A review of existing and emerging technologies,” *J Power Sources*, vol. 400, pp. 621–640, Oct. 2018, doi: 10.1016/J.JPOWSOUR.2018.08.020.
[19] P. R. Tete, M. M. Gupta, and S. S. Joshi, “Developments in battery thermal management systems for electric vehicles: A technical review,” *J Energy Storage*, vol. 35, Mar. 2021, doi: 10.1016/J.EST.2021.102255.
[20] V. Mali, R. Saxena, K. Kumar, A. Kalam, and B. Tripathi, “Review on battery thermal management systems for energy-efficient electric vehicles,” *Renewable and Sustainable Energy Reviews*, vol. 151, Nov. 2021, doi: 10.1016/J.RSER.2021.111611.
[21] Y. Liu and J. Zhang, “Design a J-type air-based battery thermal management system through surrogate-based optimization,” 2019, doi: 10.1016/j.apenergy.2019.113426.
[22] X. Na, H. Kang, T. Wang, and Y. Wang, “Reverse layered air flow for Li-ion battery thermal management,” *Appl Therm Eng*, vol. 143, pp. 257–262, Oct. 2018, doi: 10.1016/J.APPLTHERMALENG.2018.07.080.
[23] L. H. Saw, Y. Ye, A. A. O. Tay, W. T. Chong, S. H. Kuan, and M. C. Yew, “Computational fluid dynamic and thermal analysis of Lithium-ion battery pack with air cooling,” *Appl Energy*, vol. 177, pp. 783–792, Sep. 2016, doi: 10.1016/J.APENERGY.2016.05.122.
[24] S. Hong, X. Zhang, K. Chen, and S. Wang, “Design of flow configuration for parallel air-cooled battery thermal management system with secondary vent,” *Int J Heat Mass Transf*, vol. 116, pp. 1204–1212, 2018, doi: 10.1016/J.IJHEATMASSTRANSFER.2017.09.092.
[25] S. K. Mohammadian and Y. Zhang, “Thermal management optimization of an air-cooled Li-ion battery module using pin-fin heat sinks for hybrid electric vehicles,” *J Power Sources*, vol. 273, pp. 431–439, Jan. 2015, doi: 10.1016/J.JPOWSOUR.2014.09.110.
[26] X. Yu, Z. Lu, L. Zhang, L. Wei, X. Cui, and L. Jin, “Experimental study on transient thermal characteristics of stagger-arranged lithium-ion battery pack with air cooling strategy,” *Int J Heat Mass Transf*, vol. 143, Nov. 2019, doi: 10.1016/J.IJHEATMASSTRANSFER.2019.118576.
[27] K. Chen, S. Wang, M. Song, and L. Chen, “Configuration optimization of battery pack in parallel air-cooled battery thermal management system using an optimization strategy,” *Appl Therm Eng*, vol. 123, pp. 177–186, 2017, doi: 10.1016/J.APPLTHERMALENG.2017.05.060.

[28] R. W. van Gils, D. Danilov, P. H. L. Notten, M. F. M. Speetjens, and H. Nijmeijer, "Battery thermal management by boiling heat-transfer," *Energy Convers Manag*, vol. 79, pp. 9–17, Mar. 2014, doi: 10.1016/J.ENCONMAN.2013.12.006.
[29] "Heat Pipe .nl | Nederlands kenniscentrum voor heat pipe technologie | Dutch knowledge center for heat pipe technology." http://www.heatpipe.nl/index.php?page=heatpipe&lang=EN (accessed Feb. 01, 2023).
[30] "The Best Heat Transfer Fluids for Liquid Cooling." https://www.boydcorp.com/resources/temperature-control/best-heat-transfer-fluids.html (accessed Feb. 01, 2023).
[31] E. T. Mahefkey and M. M. Kreitman, "An Intercell Planar Heat Pipe for the Removal of Heat During the Cycling of a High Rate Nickel Cadmium Battery," *J Electrochem Soc*, vol. 118, no. 8, p. 1382, Aug. 1971, doi: 10.1149/1.2408330.
[32] 张国庆，吴忠杰，饶中浩，傅李鹏 and Z. G. Z. Z. Lipeng, "Experimental invesitigation on heat pipe cooling effect for power battery," 化工进展, vol. 28, no. 7, pp. 1165-, Jul. 2010, Accessed: Feb. 01, 2023. [Online]. Available: https://hgjz.cip.com.cn/CN/abstract/abstract1180.shtml
[33] G. Swanepoel, "Thermal management of hybrid electrical vehicles using heat pipes," 2001, Accessed: Feb. 01, 2023. [Online]. Available: https://www.semanticscholar.org/paper/Thermal-management-of-hybrid-electrical-vehicles-Swanepoel/bad49c7798266967419e8addf885bf55e3f7dea9#citing-papers
[34] J. Kim, J. Oh, and H. Lee, "Review on battery thermal management system for electric vehicles," *Appl Therm Eng*, vol. 149, pp. 192–212, Feb. 2019, doi: 10.1016/J.APPLTHERMALENG.2018.12.020.
[35] Y. Deng *et al.*, "Effects of different coolants and cooling strategies on the cooling performance of the power lithium ion battery system: A review," *Appl Therm Eng*, vol. 142, pp. 10–29, Sep. 2018, doi: 10.1016/J.APPLTHERMALENG.2018.06.043.
[36] C. Wang *et al.*, "Experimental examination of large capacity liFePO4 battery pack at high temperature and rapid discharge using novel liquid cooling strategy," *Int J Energy Res*, vol. 42, no. 3, pp. 1172–1182, Mar. 2018, doi: 10.1002/ER.3916.
[37] S. H. Yu, S. Sohn, J. H. Nam, and C. J. Kim, "Numerical study to examine the performance of multi-pass serpentine flow-fields for cooling plates in polymer electrolyte membrane fuel cells," *J Power Sources*, vol. 194, no. 2, pp. 697–703, Dec. 2009, doi: 10.1016/J.JPOWSOUR.2009.06.025.
[38] J. Choi, Y. H. Kim, Y. Lee, K. J. Lee, and Y. Kim, "Numerical analysis on the performance of cooling plates in a PEFC," *Journal of Mechanical Science and Technology*, vol. 22, no. 7, pp. 1417–1425, Jul. 2008, doi: 10.1007/S12206-008-0409-6/METRICS.
[39] F. C. Chen, Z. Gao, R. O. Loutfy, and M. Hecht, "Analysis of Optimal Heat Transfer in a PEM Fuel Cell Cooling Plate," *Fuel Cells*, vol. 3, no. 4, pp. 181–188, Dec. 2003, doi: 10.1002/FUCE.200330112.
[40] T. S. Fisher and K. E. Torrance, "Optimal shapes of fully embedded channels for conjugate cooling," *IEEE Transactions on Advanced Packaging*, vol. 24, no. 4, pp. 555–562, Nov. 2001, doi: 10.1109/6040.982844.
[41] T. S. Fisher and K. E. Torrance, "Constrained optimal duct shapes for conjugate laminar forced convection," *Int J Heat Mass Transf*, vol. 43, no. 1, pp. 113–126, 2000, doi: 10.1016/S0017-9310(99)00115-5.

[42] A. Jarrett and I. Y. Kim, "Design optimization of electric vehicle battery cooling plates for thermal performance," *J Power Sources*, vol. 196, no. 23, pp. 10359–10368, Dec. 2011, doi: 10.1016/J.JPOWSOUR.2011.06.090.
[43] Z. Wang *et al.*, "Thermal management investigation for lithium-ion battery module with different phase change materials," *RSC Adv*, vol. 7, no. 68, pp. 42909–42918, Sep. 2017, doi: 10.1039/C7RA08181B.
[44] S. A. Khateeb, S. Amiruddin, M. Farid, J. R. Selman, and S. Al-Hallaj, "Thermal management of Li-ion battery with phase change material for electric scooters: Experimental validation," *J Power Sources*, vol. 142, no. 1–2, pp. 345–353, Mar. 2005, doi: 10.1016/J.JPOWSOUR.2004.09.033.
[45] A. Mills and S. Al-Hallaj, "Simulation of passive thermal management system for lithium-ion battery packs," *J Power Sources*, vol. 141, no. 2, pp. 307–315, Mar. 2005, doi: 10.1016/J.JPOWSOUR.2004.09.025.
[46] R. Kizilel, A. Lateef, R. Sabbah, M. M. Farid, J. R. Selman, and S. Al-Hallaj, "Passive control of temperature excursion and uniformity in high-energy Li-ion battery packs at high current and ambient temperature," *J Power Sources*, vol. 183, no. 1, pp. 370–375, Aug. 2008, doi: 10.1016/J.JPOWSOUR.2008.04.050.
[47] L. T. Yeh and R. C. Chu, "Thermoelectric Coolers," *Thermal Management of Microelectronic Equipment*, pp. 335–347, Jul. 2002, doi: 10.1115/1.801683.CH17.
[48] "Thermoelectric Coolers | Department of Energy." https://www.energy.gov/energysaver/thermoelectric-coolers (accessed Feb. 06, 2023).
[49] Y. Liu *et al.*, "2-D mathematical modeling for a large electrochromic window - Part i," *Solar Energy Materials and Solar Cells*, vol. 120, no. PART A, pp. 1–8, 2014, doi: 10.1016/J.SOLMAT.2013.07.030.
[50] X. Wang *et al.*, "A critical review on thermal management technologies for motors in electric cars," *Appl Therm Eng*, vol. 201, Jan. 2022, doi: 10.1016/J.APPLTHERMALENG.2021.117758.
[51] Y. Yang *et al.*, "Thermal management of electric machines," *IET Electrical Systems in Transportation*, vol. 7, no. 2, pp. 104–116, Jun. 2017, doi: 10.1049/IET-EST.2015.0050.
[52] M. Grabowski, K. Urbaniec, J. Wernik, and K. J. Wołosz, "Numerical simulation and experimental verification of heat transfer from a finned housing of an electric motor," *Energy Convers Manag*, vol. 125, pp. 91–96, Oct. 2016, doi: 10.1016/J.ENCONMAN.2016.05.038.
[53] S. Ulbrich, J. Kopte, and J. Proske, "Cooling fin optimization on a TEFC electrical machine housing using a 2-D conjugate heat transfer model," *IEEE Transactions on Industrial Electronics*, vol. 65, no. 2, pp. 1711–1718, 2018, doi: 10.1109/TIE.2017.2748051.
[54] J. K. Kimotho and P. Hwang, "Thermal management of electric vehicle BLDC motor," *SAE Technical Papers*, 2011, doi: 10.4271/2011-28-0134.
[55] J. Kuria and P. Hwang, "Optimizing Heat Sink Geometry for Electric Vehicle BLDC Motor Using CFD," 2017, Accessed: Feb. 02, 2023. [Online]. Available: http://journals.jkuat.ac.ke/index.php/sri/article/viewFile/47/49
[56] C. Kim and K. S. Lee, "Thermal nexus model for the thermal characteristic analysis of an open-type air-cooled induction motor," *Appl Therm Eng*, vol. 112, pp. 1108–1116, Feb. 2017, doi: 10.1016/J.APPLTHERMALENG.2016.10.197.

[57] F. J. T. E. Ferreira, A. T. de Almeida, and M. Roffi, "Comparison of different cooling fan designs for electric motors Energy Harvesting for the IoT View project Novel Strategies in Design and Manufacturing of Energy-Efficient Motors View project Comparison of Different Cooling Fan Designs for Electric Motors," 2017, doi: 10.1109/IEMDC.2017.8002270.

[58] G. M. Gilson, S. J. Pickering, D. B. Hann, and C. Gerada, "Piezoelectric fan cooling: A novel high reliability electric machine thermal management solution," *IEEE Transactions on Industrial Electronics*, vol. 60, no. 11, pp. 4841–4851, 2013, doi: 10.1109/TIE.2012.2224081.

[59] M. S. Kim, K. S. Lee, and S. Um, "Numerical investigation and optimization of the thermal performance of a brushless DC motor," *Int J Heat Mass Transf*, vol. 52, no. 5–6, pp. 1589–1599, Feb. 2009, doi: 10.1016/J.IJHEATMASSTRANSFER.2008.07.040.

[60] T. Nakahama, K. Suzuki, S. Hashidume, F. Ishihashi, and M. Hirata, "Cooling airflow in unidirectional ventilated open-type motor for electric vehicles," *IEEE Transactions on Energy Conversion*, vol. 21, no. 3, pp. 645–651, Sep. 2006, doi: 10.1109/TEC.2006.877364.

[61] L. Song, Z. Li, J. Gao, Q. Zeng, and F. Wang, "3D thermal analysis of water cooling induction motor used for HEV | IEEE Conference Publication | IEEE Xplore," 2008. https://ieeexplore.ieee.org/document/4770758 (accessed Feb. 02, 2023).

[62] Z. Rehman and K. Seong, "Three-D Numerical Thermal Analysis of Electric Motor with Cooling Jacket," *Energies 2018, Vol. 11, Page 92*, vol. 11, no. 1, p. 92, Jan. 2018, doi: 10.3390/EN11010092.

[63] M. Satrústegui, M. Martinez-Iturralde, J. C. Ramos, P. Gonzalez, G. Astarbe, and I. Elosegui, "Design criteria for water cooled systems of induction machines," *Appl Therm Eng*, vol. 114, pp. 1018–1028, 2017, doi: 10.1016/J.APPLTHERMALENG.2016.12.031.

[64] P. S. Wu *et al.*, "Heat Transfer and Thermal Management of Interior Permanent Magnet Synchronous Electric Motor," *Inventions 2019, Vol. 4, Page 69*, vol. 4, no. 4, p. 69, Nov. 2019, doi: 10.3390/INVENTIONS4040069.

[65] C. Li, Z. Guan, J. Li, B. Zhao, and X. Ding, "Optimal design of cooling system for water cooling motor used for mini electric vehicle," *2017 20th International Conference on Electrical Machines and Systems, ICEMS 2017*, Oct. 2017, doi: 10.1109/ICEMS.2017.8056319.

[66] A. Deriszadeh, F. de Monte, M. Villani, and L. di Leonardo, "Hydrothermal performance of ethylene glycol and water mixture in a spiral channel for electric motor cooling," *2019 21st European Conference on Power Electronics and Applications, EPE 2019 ECCE Europe*, Sep. 2019, doi: 10.23919/EPE.2019.8914967.

[67] C. Yang, H. Wang, X. Niu, J. Zhang, and Y. Yan, "Design and Analysis of Cycling Oil Cooling in Driving Motors for Electric Vehicle Application," *2016 IEEE Vehicle Power and Propulsion Conference, VPPC 2016 - Proceedings*, Dec. 2016, doi: 10.1109/VPPC.2016.7791651.

[68] A. Acquaviva, S. Skoog, and T. Thiringer, "Design and Verification of In-Slot Oil-Cooled Tooth Coil Winding PM Machine for Traction Application," *IEEE Transactions on Industrial Electronics*, vol. 68, no. 5, pp. 3719–3727, May 2021, doi: 10.1109/TIE.2020.2985009.

[69] S. A. Semidey and J. R. Mayor, “Experimentation of an electric machine technology demonstrator incorporating direct winding heat exchangers,” *IEEE Transactions on Industrial Electronics*, vol. 61, no. 10, pp. 5771–5778, 2014, doi: 10.1109/TIE.2014.2303779.

[70] P. Lindh, I. Petrov, J. Pyrhonen, E. Scherman, M. Niemela, and P. Immonen, “Direct Liquid Cooling Method Verified with a Permanent-Magnet Traction Motor in a Bus,” *IEEE Trans Ind Appl*, vol. 55, no. 4, pp. 4183–4191, Jul. 2019, doi: 10.1109/TIA.2019.2908801.

[71] A. Reinap, F. J. Marquez-Fernandez, M. Alakula, R. Deodhar, and K. Mishima, “Direct Conductor Cooling in Concentrated Windings,” *Proceedings - 2018 23rd International Conference on Electrical Machines, ICEM 2018*, pp. 2654–2660, Oct. 2018, doi: 10.1109/ICELMACH.2018.8507094.

[72] Z. Xu *et al.*, “Thermal management of a permanent magnet motor for an directly coupled pump,” *Proceedings - 2016 22nd International Conference on Electrical Machines, ICEM 2016*, pp. 2738–2744, Nov. 2016, doi: 10.1109/ICELMACH.2016.7732909.

[73] A. Tüysüz *et al.*, “Advanced Cooling Methods for High-Speed Electrical Machines,” *IEEE Trans Ind Appl*, vol. 53, no. 3, pp. 2077–750, doi: 10.1109/TIA.2017.2672921.

[74] M. Schiefer and M. Doppelbauer, “Indirect slot cooling for high-power-density machines with concentrated winding,” *Proceedings - 2015 IEEE International Electric Machines and Drives Conference, IEMDC 2015*, pp. 1820–1825, Feb. 2016, doi: 10.1109/IEMDC.2015.7409311.

[75] Y. Alexandrova, R. S. Semken, and J. Pyrhönen, “Permanent magnet synchronous generator design solution for large direct-drive wind turbines: Thermal behavior of the LC DD-PMSG,” *Appl Therm Eng*, vol. 65, no. 1–2, pp. 554–563, Apr. 2014, doi: 10.1016/J.APPLTHERMALENG.2014.01.054.

[76] X. Chen, J. Wang, A. Griffo, and A. Spagnolo, “Thermal Modeling of Hollow Conductors for Direct Cooling of Electrical Machines,” *IEEE Transactions on Industrial Electronics*, vol. 67, no. 2, pp. 895–905, Feb. 2020, doi: 10.1109/TIE.2019.2899542.

[77] A. Reinap, M. Andersson, F. J. Márquez-Fernández, P. Abrahamsson, and M. Alaküla, “Performance Estimation of a Traction Machine with Direct Cooled Hairpin Winding,” *ITEC 2019 - 2019 IEEE Transportation Electrification Conference and Expo*, Jun. 2019, doi: 10.1109/ITEC.2019.8790545.

[78] V. Madonna, A. Walker, P. Giangrande, G. Serra, C. Gerada, and M. Galea, “Improved thermal management and analysis for stator end-windings of electrical machines,” *IEEE Transactions on Industrial Electronics*, vol. 66, no. 7, pp. 5057–5069, Jul. 2019, doi: 10.1109/TIE.2018.2868288.

[79] V. Madonna, P. Giangrande, A. Walker, and M. Galea, “On the Effects of Advanced End-Winding Cooling on the Design and Performance of Electrical Machines,” *Proceedings - 2018 23rd International Conference on Electrical Machines, ICEM 2018*, pp. 311–317, Oct. 2018, doi: 10.1109/ICELMACH.2018.8507170.

[80] F. Marcolini, G. de Donato, and F. Caricchi, “Direct oil cooling of end-windings in torus-type axial-flux permanent-magnet machines,” *2019 IEEE Energy Conversion Congress and Exposition, ECCE 2019*, pp. 5645–5651, Sep. 2019, doi: 10.1109/ECCE.2019.8912993.

[81] G. Liang and I. Mudawar, “Review of spray cooling – Part 1: Single-phase and nucleate boiling regimes, and critical heat flux,” *Int J Heat Mass Transf*, vol. 115, pp. 1174–1205, Dec. 2017, doi: 10.1016/J.IJHEATMASSTRANSFER.2017.06.029.

[82] T. Davin, J. Pellé, S. Harmand, and R. Yu, “Experimental study of oil cooling systems for electric motors,” *Appl Therm Eng*, vol. 75, pp. 1–13, Jan. 2015, doi: 10.1016/J.APPLTHERMALENG.2014.10.060.

[83] L. Ye, F. Tao, L. Qi, and W. Xuhui, “Experimental investigation on heat transfer of directly-oil-cooled permanent magnet motor,” 2016, Accessed: Feb. 02, 2023. [Online]. Available: https://ieeexplore.ieee.org/abstract/document/7837110

[84] C. Liu *et al.*, “Experimental Investigation on Oil Spray Cooling with Hairpin Windings,” *IEEE Transactions on Industrial Electronics*, vol. 67, no. 9, pp. 7343–7353, Sep. 2020, doi: 10.1109/TIE.2019.2942563.

[85] S. la Rocca *et al.*, “Numerical study of the impact of different cooling arrangements on a high length/diameter ratio motor for electric commercial vehicle,” *Proceedings - ICOECS 2019: 2019 International Conference on Electrotechnical Complexes and Systems*, Oct. 2019, doi: 10.1109/ICOECS46375.2019.8949929.

[86] “BLDC / PMSM brushless motor HPM-10KW - Nominal power10kW~13kW | 13,4AG~17,4AG | 650cm3 - Brushless BLDC motor with permanent magnet - Miromax - EMPOWERING SOLUTIONS.” https://www.miromax.lt/en/c-39/c-45-brushless_bldc_motor_with_permanent_magnet/product-507-bldc__pmsm_brushless_motor_hpm-10kw_-_nominal_power10kw13kw__134ag174ag___650cm3#product (accessed Feb. 06, 2023).

ANNEX A

A1. BATTERY

Item	Parameter
Cell model	3.2V105Ah
Cell type	LFP
Cell nominal capacity	105Ah
Cell nominal voltage	3.2V
Working voltage	2.5~3.65V
Cell weight	2.06kg
Cell energy density	163Wh/kg
Max. charging current	1C
Max. discharge current	2C
ACR	≤0.7mΩ
Battery working temp.	Discharging:-20℃~55℃ Charging:0~55℃

Figure A.1 - Battery specifications

A2. TOOL MOTOR

Items NO.	Voltage V	Current A	P.input W	P. factor PF	Frequency Hz	Torque mN.m	Rotate Rpm	P.output W	Efficiency %
1	71.83	7.297	524.11	1.000	0.00	468.0	4659	228.32	43.6
2	71.82	7.606	546.28	1.000	0.00	357.5	4658	174.37	31.9
3	71.81	9.103	653.73	1.000	0.00	147.5	4647	71.77	11.0
4	71.79	12.522	898.97	1.000	0.00	805.0	4621	389.52	43.3
5	71.75	18.159	1302.97	1.000	0.00	1917.5	4580	919.60	70.6
6	71.70	25.740	1845.49	1.000	0.00	3242.5	4525	1536.37	83.3
7	71.64	34.868	2497.87	1.000	0.00	4772.5	4460	2228.83	89.2
8	71.58	45.202	3235.65	1.000	0.00	6460.0	4388	2968.22	91.7
9	71.52	56.724	4056.79	1.000	0.00	8327.5	4320	3766.99	92.9
10	71.45	68.855	4919.31	1.000	0.00	10315.0	4251	4591.53	93.3
11	71.38	81.549	5820.60	1.000	0.00	12427.5	4181	5440.77	93.5
12	71.30	94.671	6750.04	1.000	0.00	14587.5	4114	6284.08	93.1
13	71.23	107.898	7685.30	1.000	0.00	16797.5	4052	7127.06	92.7
14	71.21	121.197	8630.78	1.000	0.00	18967.5	3996	7936.56	92.0
15	71.27	134.038	9552.52	1.000	0.00	21112.5	3949	8730.18	91.4
16	71.30	146.140	10419.78	1.000	0.00	23077.5	3910	9448.48	90.7
17	71.26	156.545	11155.40	1.000	0.00	24825.0	3872	10065.17	90.2
18	71.22	165.043	11754.33	1.000	0.00	26172.5	3842	10529.29	89.6
19	71.24	171.080	12187.74	1.000	0.00	27107.5	3825	10857.19	89.1
20	71.27	175.565	12512.52	1.000	0.00	27762.5	3816	11093.37	88.7
21	71.29	178.693	12738.54	1.000	0.00	28297.5	3809	11286.41	88.6
22	71.30	181.525	12942.28	1.000	0.00	28692.5	3803	11425.92	88.3
23	71.34	184.110	13134.41	1.000	0.00	29087.5	3800	11574.08	88.1
24	71.34	186.195	13284.08	1.000	0.00	29415.0	3797	11695.16	88.0
25	71.34	188.323	13433.99	1.000	0.00	29770.0	3791	11817.60	88.0
26	71.33	190.278	13572.49	1.000	0.00	30065.0	3787	11922.11	87.8
27	71.34	192.378	13724.21	1.000	0.00	30357.5	3783	12025.38	87.6
28	71.32	194.243	13854.35	1.000	0.00	30627.5	3779	12119.51	87.5

Figure A.2 - Tool motor specifications

A3. TRACTION MOTOR

PROPOSED DATA					
Gearbox type			**701C2**		
Gearbox ratio	(i)		30,0		
Gearbox efficiency			0,94		
Brake type			**Parking Electromagnetic**		
Brake torque	(Nm)		70		
Brake Voltage supply	(Vdc)		TBC		
Brake torque at the sprocket	(Nm)		2232		
Motor			**VSDMOT-SW02**		
Rated Power	(kW)		7,5		
Rated Torque	(Nm)		32		
Rated Speed	(rpm)		2250		
Rated Current	(Arms)		100		
Rated Voltage	(Vrms)		53		
Rated Frequency	(Hz)		150		
Bus-DC Voltage	(Vdc)		80		
Working Points					
Type of service		S2-10'	S2-10'	S2-60'	
Motor torque	(Nm)	21	76	32	
Motor speed	(rpm)	4.883	723	1.809	
Motor power	(kW)	10,7	5,7	6,1	
Motor supply voltage	(Vrms)	14	15	17	
Motor supply current	(Arms)	190	175	250	
cosφ	(p.u.)	0,88	0,89	0,84	
Efficiency	(%)	85	88	84	
Degree of protection			IP67		
Sprocket torque	(Nm)	589	2.135	904	
Sprocket speed	(rpm)	162,8	24,1	60,3	
Max. tractive effort	(N)	4.550	16.499	6.983	
Travel speed	**(km/h)**	**13,5**	2,0	**5,0**	
Max. gradeability	**(%)**	3,0	**40,0**	**10,0**	
Gearbox effic. μg = 0,94 - Track effic. μt = 0,85 - Rolling resist. rr= 0,10					

Figure A.3 - Traction motor specifications

A4. Dissipation values for each component

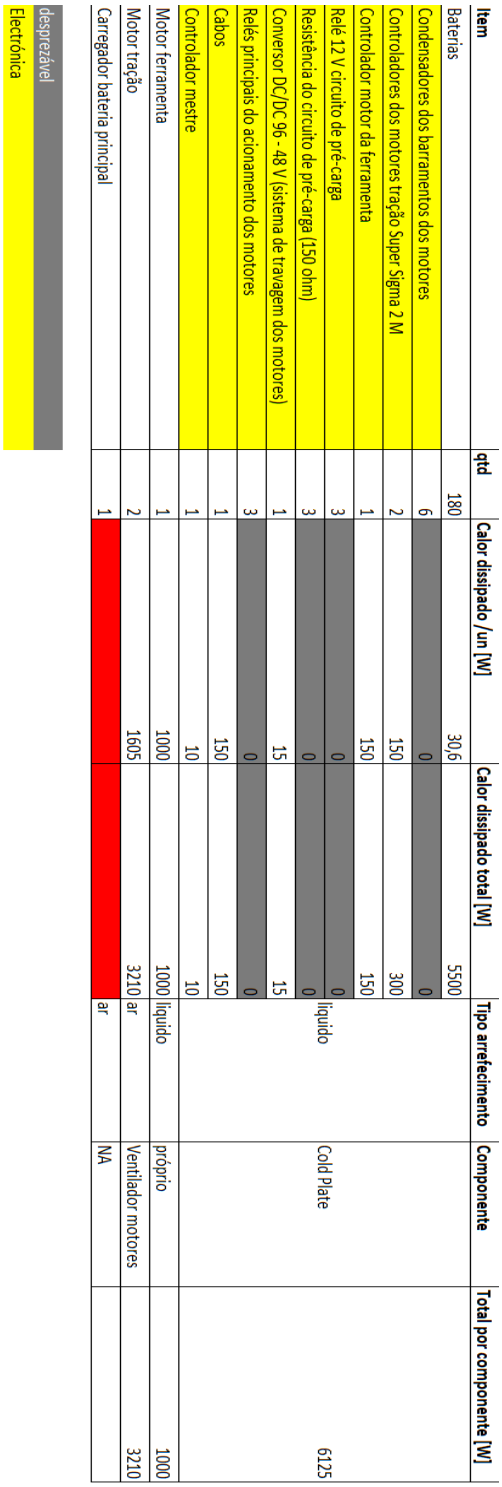

Item	qtd	Calor dissipado /un [W]	Calor dissipado total [W]	Tipo arrefecimento	Componente	Total por componente [W]
Baterias	180	30,6	5500			
Condensadores dos barramentos dos motores	6	0	0			
Controladores dos motores tração Super Sigma 2 M	2	150	300			
Controlador motor da ferramenta	1	150	150			
Relé 12 V circuito de pré-carga	3	0	0	liquido	Cold Plate	6125
Resistência do circuito de pré-carga (150 ohm)	3	0	0			
Conversor DC/DC 96 - 48 V (sistema de travagem dos motores)	1	15	15			
Relés principais do acionamento dos motores	3	0	0			
Cabos	1	150	150			
Controlador mestre	1	10	10			
Motor ferramenta	1	1000	1000	liquido	próprio	1000
Motor tração	2	1605	3210	ar	Ventilador motores	3210
Carregador bateria principal	1			ar	NA	

desprezável
Electrónica

Figure A.4 - Dissipation values per component

A5. PUMP

Name	**HIGH FLOW SYSTEM 12 VDC 10.0 GPM**
Model Numbers OEM/Aftermarket	4558-153-E75
Voltage	12 VDC
Dimensions Inches/Millimeters	
Flow Rate GPM/LPM	10.0 GPM [37.8 LPM]
Amps (Max.)	13/11
Shut-Off Pressure	55 PSI [3.8 BAR]

Figure A.5 - Pump specifications

A6. CHECK VALVE

Technical specifications

series	3045-3046	3047-3048-3041
Materials		
Body:	brass EN 12165 CW617N	brass EN 12165 CW617N
Check valve:	POM	POM
Springs:	stainless steel	stainless steel
O-Ring seals:	EPDM, NBR	EPDM, NBR
Union seal:	3046 series: non-asbestos fibre NBR	3041 series: non-asbestos fibre NBR
Knob:	-	3041 series: EN 12165 CW617N
Ball:	-	3041 series: EN 12164 CW614N, chrome-plated
Ball control stem:	-	3041 series: EN 12164 CW614N
Ball seal seat:	-	3041 series: PTFE
Test port cap:	3045/3046 series PA66G30; code 304601: brass EN 12164 CW614N	3048/3041 series: PA66G30
Performance		
Medium:	drinking water	drinking water
Maximum working pressure:	10 bar	10 bar
Min. opening pressure for check valve:	0,5 kPa	0,5 kPa
Maximum working temperature:	90°C	90°C
Connections (internal check valve DN)	3045 series: 1/2" 2" F (DN 15 50) code 304601: 3/4" F with union for M (DN 15) 3046 series: 3/4" 2" F with union for M (DN 15 40) code 304644: 3/4" F with captive nut for M (DN 15) code 304654: 1" F with captive nut for M (DN 20) code 304645: 3/4" F with captive nut for M (DN 15)	3047 series: 1/2" 1" F (DN 15 25) 3048 series: 1/2", 3/4" F (DN 15, 20) 3041 series: 3/4" F with union for M (DN 15)
Test port connections	1/4" F; code 304601: 1/8" F	3048/3041 series: 1/4" F

Hydraulic characteristics

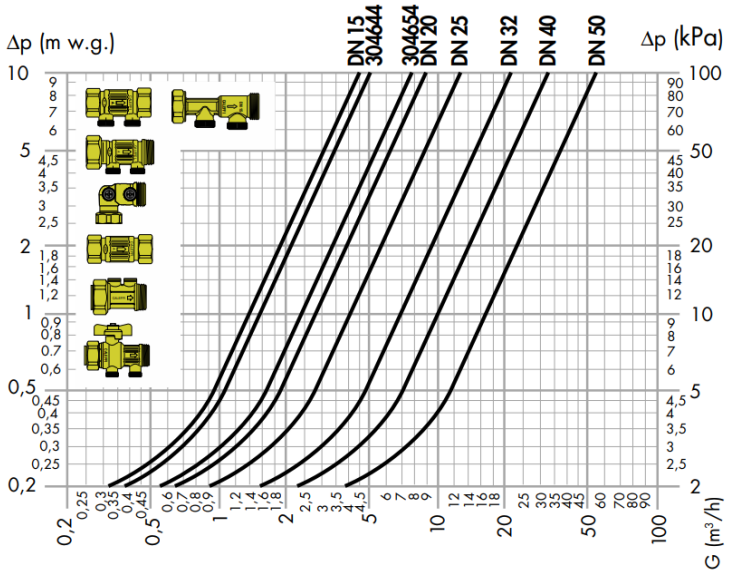

Figure A.6 - Check valve specifications

A7. 2-WAY AND 3-WAY VALVE

ATUADORES De pequena dimensão	TERMOELÉTRICO, ação modulante (0-10 VCC)	ELÉTRICO ação modulante (0-10 VCC)	TERMOELÉTRICO ação tudo/nada ou DAT
Grau de protecção	IP54 (norma EN 60529)	IP43 (norma EN 60529)	P54 (norma EN 60529)
Força nominal	125N ± 5%	120N	100N + 5%
Alimentação	24 VCA (± 10%)	24 VCA/CC (± 10%)	230 VCA (ou 24 VCA/CC) ± 10%
Sinal de comando	0 a 10 VCC (Ri ≥ 100 kΩ)	0 a 10 VCC (Ri ≥ 100 kΩ) ou 3 pontos (reversível)	-----
Característica	Linear	linear ou igual percentagem (comutável)	-----
Tempo de abertura/fecho	2,5 minutos	40 seg	3 minutos
Consumo (potência)	1,2W (máx. 320 mA)	1,5W	1W («Pico inicial» (0,1 seg) 100W/230 VCA); 7W 24 VCA/CC
Ligações (cabo)	com 1 m de comprimento; 3 condutores de 0,75mm²	com 1,5 m de comprimento; 3 condutores de 0,75mm²	com 1 m de comprimento; 2 condutores de 0,75mm²
Temperatura ambiente	0 ... 60ºC		
Humidade relativa	≤ 95%H		
Certificados (CE)	EEC EMC (CEI-EN 55104/95; CEI-EN 55104/00; EN 60730-1; EN 60730-2-14		

VÁLVULAS DE LIGAÇÕES ROSCADAS MACHO/MACHO					VÁLVULA + ATUADOR		
Kvs	ΔP (1) MÁXIMO	CAUDAL (2) MÁXIMO RECOMENDADO	LIGAÇÕES HIDRÁULICAS	CÓDIGO ENCOMENDA	COMBINAÇÃO POSSÍVEL		
VÁLVULAS DE 2 VIAS							
2,5	250 kPa	1.000 l/h	1/2"	VG 3210 FS	✓	✓	✓
4,0	200 kPa	1.600 l/h	3/4"	VG 3210 KS	✓	✓	✓
6,3	100 kPa	2.500 l/h	1"	VG 3210 LS	✓	✓	✓
VÁLVULAS DE 3 VIAS							
2,5	250 kPa	1.000 l/h	1/2"	VG 3310 FS	✓	✓	✓
4,0	200 kPa	1.600 l/h	3/4"	VG 3310 KS	✓	✓	✓
6,3	100 kPa	2.500 l/h	1"	VG 3310 LS	✓	✓	✓
VÁLVULAS DE 4 VIAS							
2,5	250 kPa	1.000 l/h	1/2"	VG 3410 FS	✓	✓	✓
4,0	200 kPa	1.600 l/h	3/4"	VG 3410 KS	✓	✓	✓
6,3	100 kPa	2.500 l/h	1"	VG 3410 LS	✓	✓	✓

Figure A.7 - 2 and 3-way valves specifications

A8. THERMOSTATIC VALVE

Características técnicas

- Material:	- Corpo:	Latão UNI EN 12165 CW617N, cromado
	- Cartucho:	Latão UNI EN 12164 CW614N
	- Obturador:	Latão UNI EN 12164 CW614N
	- Molas:	Aço inox
	- Elementos de vedação:	NBR
Fluido de utilização:		água

Campo de regulação:	30÷65°C
Precisão:	±2°C
Pressão máx. exercício (estática):	14 bar
Pressão máx. exercício (dinâmica):	5 bar
Temperatura máx. de entrada:	85°C
Relação máxima entre as pressões de entrada (Q/F o F/Q):	2:1
Ligação:	- 1"÷2" M de casquilho -Ø 28 mm para tubo de cobre

Características hidráulicas

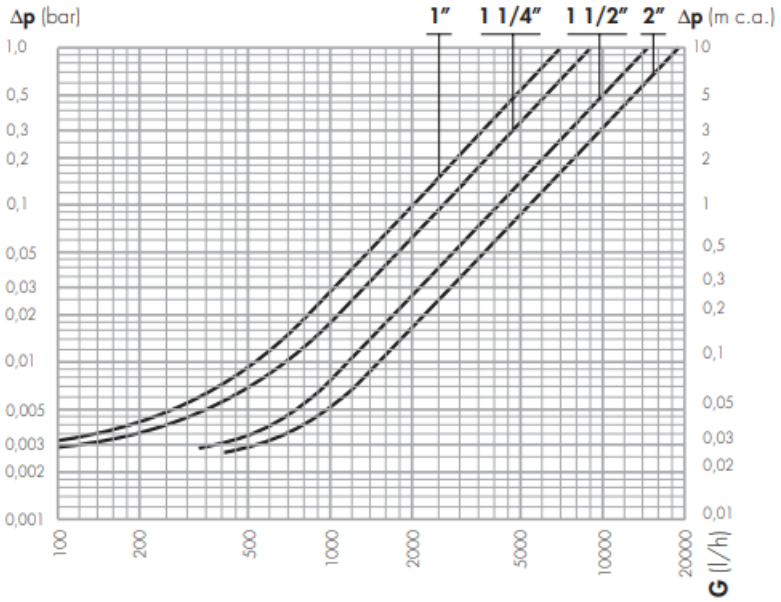

Figure A.8 - Thermostatic valve specifications

A9. SECTIONING VALVE

série ⇨		3230 - 332 - 333 - 334
Materiais		
Corpo:		latão UNI EN 12165 CW617N, cromado
Esfera:	medidas 1/2"÷1"	latão UNI EN 12164 CW614N, cromado
	medidas 1 1/4"÷2"	latão UNI EN 12165 CW617N, cromado
Retenção:	medida 1/2"	PA
	medida 3/4"	POM
	medidas 1"-1 1/4"	PSU
	medidas 1 1/2"-2"	latão UNI EN 12164 CW614N, cromado
Mola de retenção:		aço inoxidável
Vedação da retenção:		NBR
Manípulos de comando (alavanca/borboleta):		alumínio
Vedação da haste de comando:		PTFE
Desempenho		
Fluido de utilização:		água, hidrocarbonetos
Percentagem máx. de glicol:		-
Pressão máx. de funcionamento:		16 bar
Pressão mínima de abertura da retenção (Δp):		0,02 bar
Campo de temperatura de funcionamento:		5÷90°C
Ligações		Série 3230: 1/2"÷2" F
		Código 332400: 1/2" M x 1/2" F
		Código 333400: 1/2" F x porca 3/4" F
		Código 333500: 3/4" F x porca 3/4" F
		Código 334400: 1/2" M x porca 3/4" F
		Código 334500: 3/4" M x porca 3/4" F
		Série 333 e 334: porca com furação para selagem

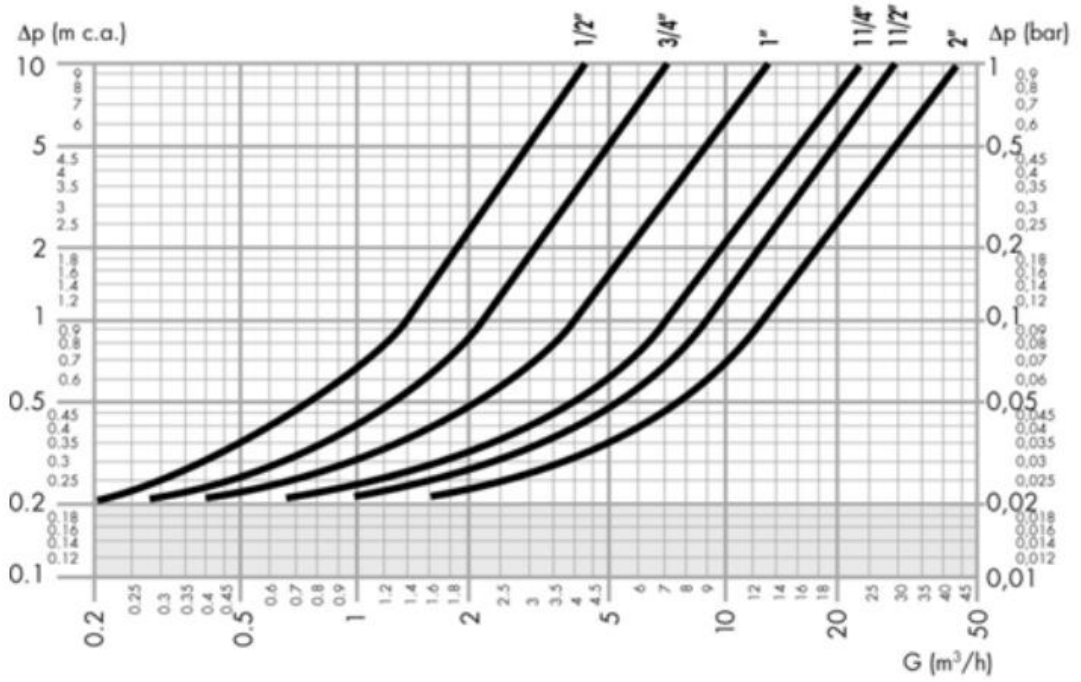

Figure A.9 - Sectioning valve specifications

A10. TEMPERATURE SENSOR

technical data	
measuring element:	Platinum resistance element Pt100
measuring temperature:	up to 140°C
tolerance:	class A, according IEC 60751
signal type:	1x Pt100 in 4-wire-switch 4...20 mA / 20...4 mA with line transmitter LTN-500
installation:	contact sensor with special clamp
connection:	Silikon/PTFE shielded cable, others on request
materials	
Messfläche:	Ag
sensor housing:	Polyamid
clamp:	POM; others on request
protection class:	IP68

Figure A.10 - Temperature sensor specifications

A11. RADIATOR FAN

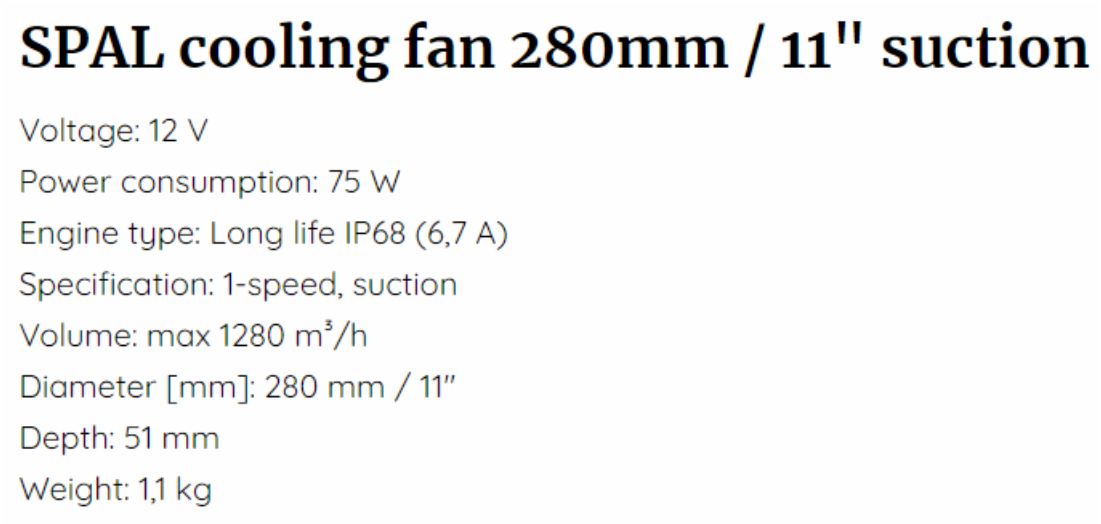

Figure A.11 - Radiator fan specifications